PHYSICAL REVIEW B VOLUME 54, NUMBER 19 15 NOVEMBER 1996-I

Theory of anyon excitons: Relation to excitons of $\nu=1/3$ and $\nu=2/3$ incompressible liquids

M. E. Portnoi
Department of Physics, University of Utah, Salt Lake City, Utah 84112
and A. F. Ioffe Institute, St. Petersburg 194021, Russia

E. I. Rashba
Department of Physics, University of Utah, Salt Lake City, Utah 84112
and L. D. Landau Institute for Theoretical Physics, Moscow 117940, Russia

(Received 16 May 1996)

Elementary excitations of incompressible quantum liquids (IQL's) are anyons, i.e., quasiparticles carrying fractional charges and obeying fractional statistics. To find out how the properties of these exotic quasiparticles manifest themselves in the optical spectra, we have developed the anyon-exciton model (AEM) and compared the results with the finite-size data for excitons of $\nu=1/3$ and $\nu=2/3$ IQL's. The model considers an exciton as a neutral composite consisting of three quasielectrons and a single hole. The AEM works well when the separation between electron and hole confinement planes, h, obeys the condition $h\gtrsim 2l$, where l is the magnetic length. In the framework of the AEM an exciton possesses momentum $\mathbf{k}$ and two internal quantum numbers, one of which can be chosen as the angular momentum L of the $\mathbf{k}=0$ state. Charge fractionalization manifests itself in striking differences between the properties of anyon excitons and ordinary magnetoexcitons. The existence of the internal degrees of freedom results in the multiple-branch energy spectrum, craterlike electron density shape, and 120° density correlations for $\mathbf{k}=0$ excitons, and the splitting of the electron shell into bunches for $\mathbf{k}\neq 0$ excitons. For $h\gtrsim 2l$ the bottom states obey the superselection rule $L=3m$, where $m\geqslant 2$ are integers, and all of them are hard-core states. For $h\approx 2l$ there is one-to-one correspondence between the low-energy spectra found for the AEM and the many-electron exciton spectra of the $\nu=2/3$ IQL, whereas some states are absent from the many-electron spectra of the $\nu=1/3$ IQL. We argue that this striking difference in the spectra originates from the different populational statistics of the quasielectrons of charge conjugate IQL's and show that the proper account of the statistical requirements eliminates excessive states from the spectrum. Apparently, this phenomenon is the first manifestation of the exclusion statistics in the anyon bound states. [S0163-1829(96)07643-6]

I. INTRODUCTION

Incompressible quantum liquids[1] (IQL's) underlie the fractional quantum Hall effect (FQHE) discovered by Tsui, Stormer, and Gossard.[2] The charge carriers in these liquids are anyons, i.e., quasiparticles (quasielectrons and quasiholes) carrying fractional charges[1] and obeying fractional statistics.[3,4] Historically the main experimental discoveries in this field were done by magnetotransport experiments. However, the role of spectroscopic methods is continuously increasing since they provide an indispensable tool for investigating spectra of elementary excitations. Fine structure specific for different electronic phases was discovered in the spectra of radiative photoemission.[5] These spectra were used to measure gaps in the energy spectra of IQL's, for investigation of phase transitions between the IQL and Wigner solid phases, etc. The frequency of long-wave neutral elementary excitations of IQL's was measured in Raman scattering experiments.[6]

A challenging problem in physics of IQL's is a direct observation of the charge fractionalization. Between different exciting approaches to this problem the spectroscopic approach seems to be one of the most promising. Indeed, spectroscopy permits one to observe properties of IQL's in the bulk where the effect of the impurities and edges is reduced to the minimum. The intrinsic spectroscopy of IQL's is the magnetospectroscopy of excitons. However, properties of excitons reflect the spectrum of the elementary excitations of an IQL (quasielectrons and quasiholes, magnetorotons,[7] etc.) and can be treated in terms of them only when the separation h between electron and hole confinement planes is sufficiently large. Indeed, when $h\lesssim l$, where l is the magnetic length, the filling factor ν of the liquid strongly deviates in the vicinity of the hole from the quantized value $\nu=p/q$. Under these conditions the properties of the IQL cannot be treated in terms of its quasiparticles. The spectroscopy of a remote hole has been discussed from different standpoints in a number of papers.[8–12] Despite the fact that experiments in the $h\gg l$ region are rather complicated, the separations up to $h\approx 5l$ were achieved in experiments on extrinsic radiative photoemission.[13] Of special importance might be experiments performed for a fixed filling factor $\nu=p/q$ and a variable dimensionless electron-hole separation h/l.[14] The first experiments of this kind were reported recently.[15]

The investigation of excitons is also important from the different standpoint. In the theory of IQL's the statistical properties of the system of free anyons are usually discussed. In an exciton the anyons exist in a bound state because of the attracting potential of a hole. It was shown[16,17] that the energy spectra of excitons of $\nu=1/3$ and $\nu=2/3$ IQL's are

closely related to the statistical and dynamical properties of quasielectrons of these IQL's. Therefore, the exciton problem can be really treated as a few-anyon problem. Excitons represent a wide class of few-anyon systems. It includes excitons, anyon ions[18,19] (which can be also treated as quasiparticle-exciton complexes[20]), some impurity centers, etc. In what follows, we consider excitons as bound few-anyon composites and investigate their properties in some detail.

There are two approaches to the theory of excitons in IQL's. The first approach is based on the exact diagonalization for finite-size systems in the spherical geometry.[21] Having in mind workable system sizes, it provides reliable results for $h \lesssim 2l$, at least as applied to the $\nu=1/3$ and $\nu=2/3$ IQL's. The second approach is based on the anyon-exciton model (AEM) proposed by the present authors.[11,22] In the framework of this approach an exciton is considered as a neutral composite quasiparticle consisting of several anyons and a hole. This model is exact only when the exciton size which is about h is large compared to the size of anyons which is about l, i.e., for $h/l \gg 1$. Therefore, the two approaches are complementary and one can expect that they match when $h/l \sim 1$.

It is the main statement of the AEM that excitons of IQL's possess a multiple-branch spectrum. Indeed, a charged particle at the lowest Landau level possesses a single degree of freedom and a single quantum number. An exciton being a neutral entity possesses in a magnetic field a vector momentum $\mathbf{k}$ absorbing two degrees of freedom.[23] Therefore, an exciton consisting of q anyons and a hole possesses $q-1$ internal degrees of freedom. For an ordinary magnetoexciton $q=1$ and the spectrum consists of a single-branch. For $q \geqslant 2$ an exciton acquires internal quantum number(s) and multiple-branch spectrum. This prediction of the AEM permitted Apalkov *et al.*[16,17,24] to represent the energy spectra found by finite-size computations for $\nu=1/3$ and $\nu=2/3$ IQL's as a system of exciton-branches and to assign to these branches internal quantum numbers. The latter determine the values of the exciton angular momentum L in the $\mathbf{k}=0$ states. Zang and Birman[25] and Chen and Quinn[26] also inferred the existence of several exciton branches in their finite-size data.

In the range accessible for finite-size studies, $h \lesssim 2l$, there are two types of excitons in the lower part of the energy spectrum, anyon excitons and tight excitons. *Anyon excitons* are loose entities with a pronounced anyon-density dip at the center. They are generically related to the quantum states making up the low-energy (anyon) sector[27,28] of the electron subsystem. Each anyon exciton is a bound state of a three-quasielectron complex from the anyon sector and a hole. This finding establishes a connection between the spectroscopy of excitons and the low-energy physics of the FQHE. There is a striking difference in the quantum numbers of the low-energy anyon-excitons of the $\nu=1/3$ and $\nu=2/3$ IQL's. It is related to the difference in the energy spectra of the three-quasielectron complexes originating due to the different populational statistics of the quasielectrons of these liquids. *Tight excitons* are dense entities. A sharp density maximum is achieved either in the center of an exciton or in a close vicinity of the center. These excitons are not related to the low-energy sector of the electron subsystem. The $L=0$ tight exciton is the bottom state of the exciton spectrum in all the region $h \lesssim 2l$. Therefore, the $h \gtrsim 2l$ region seems to be of the most importance for the study of the anyon substructure of excitons and for the spectroscopic observation of the charge fractionalization.

We suppose everywhere in this paper that the spin-polarized background is stable with respect to formation of charged spin textures (skyrmions). It was predicted recently[29] that spin textures develop in the ground state of a $\nu=1$ exciton for large values of h/l; the critical value of h/l is about 1.5 for GaAs. Nevertheless, we feel that the spin-polarized ground state of a $\nu=1/3$ magnetoexciton is stable because skyrmions can exist only at very low magnetic fields when $\nu \approx 1/3$.[30] Spin-depolarized excitons should be seen in the spectrum of excited states.

In this paper we develop the theory of excitons in the framework of the AEM as applied to excitons consisting of three quasielectrons and a hole. We use Halperin pseudo-wave-functions[3] in a boson basis and investigate the energy spectrum, electron density distribution, and anyon correlations in an exciton. We make comparison with the finite-size data[16,17] on the excitons of the $\nu=1/3$ and $\nu=2/3$ IQL's and conclude that excitons of the $\nu=2/3$ IQL are described rather well by the AEM because of the bosonic populational statistics and the narrow form factors of the quasielectrons of this liquid. We also relate the difference in the energy spectra of the anyon excitons of the $\nu=1/3$ and $\nu=2/3$ IQL's to some specific features in the exciton shape found in the framework of the AEM. For both IQL's the bottom exciton states are made by tight $L=0$ excitons for $h \lesssim 2l$ and by a succession of anyon excitons for $h \gtrsim 2l$. This succession consists of hard-core excitons with the angular momenta L which are integers of 3 and increase as $L \propto h^2$ with h.

The general outline of the paper is as follows. In Sec. II we construct a full basis of the exciton wave functions for the AEM using the translational symmetry and permutation symmetry arguments. In Sec. III we develop a technique for calculating different matrix elements entering the Schrödinger equation. In Secs. IV, V, and VI we obtain energy spectra, electron density distributions, and the density correlation functions, respectively. The latter functions unveil the anyon substructure of excitons both in the finite-size data and in the AEM. In Sec.VII we make a comparison of the results obtained in the framework of the AEM with finite-size data of Refs. 16 and 17. We propose that a striking difference in the finite-size data for the $\nu=1/3$ and $\nu=2/3$ IQL's originates from the difference in the populational statistics of the quasielectrons of these liquids.

II. WAVE FUNCTIONS

Let us consider an exciton consisting of a valence hole with a charge $(+e)$ and three QE's with electrical charges $(-e/3)$ and statistical charges α. Such an entity provides the AEM description of the anyon excitons of the $\nu=1/3$ and $\nu=2/3$ IQL's. For an $\nu=1/3$ IQL the statistical charge equals $\alpha=-1/3$, while for a $\nu=2/3$ IQL the statistical charge has the same value, $\alpha=1/3$, as for quasiholes in a $\nu=1/3$ IQL.[3] In comparison, $\alpha=0$ for bosons and $\alpha=1$ for fermions. In the strong magnetic field limit, when the Cou-

lomb energy $\varepsilon_C = e^2/\epsilon l \ll \hbar\omega_c$, where ω_c is the cyclotron frequency and ε is the dielectric constant, it is convenient to employ dimensionless variables scaled in units ε_C, l, and e. We use the symmetric gauge, $\mathbf{A}=\hat{z}\times\mathbf{r}/2$, where $\hat{z}$ is a unit vector perpendicular to the confinement plane. Instead of the hole, $\mathbf{r}_h$, and anyon, $\mathbf{r}_i$, coordinates it is convenient to introduce the following two-dimensional (2D) coordinates:

$$\mathbf{R}=\frac{1}{2}\left(\mathbf{r}_h+\frac{1}{3}\sum_{i=1}^{3}\mathbf{r}_i\right),\quad \boldsymbol{\rho}=\frac{1}{3}\sum_{j=1}^{3}\mathbf{r}_j-\mathbf{r}_h,\quad \mathbf{r}_{jl}=\mathbf{r}_j-\mathbf{r}_l,$$
$$jl=12,\ 23,\ \text{and}\ 31. \tag{1}$$

$\mathbf{R}$ has a meaning of the center-of-mass of the exciton coordinate. The coordinates $\boldsymbol{\rho}$ and $\mathbf{r}_{jl}$ are the internal variables which are not affected by the translational motion of an exciton. Complex coordinates $z_{jl}=x_{jl}+iy_{jl}$, as well as $\mathbf{r}_{jl}$, are not independent. Indeed,

$$\mathbf{r}_{12}+\mathbf{r}_{23}+\mathbf{r}_{31}=0. \tag{2}$$

Despite the fact that the constraint (2) results in some complications, the introduction of the variables $\mathbf{r}_{jl}$ enables one to develop the theory in a form symmetric in all anyons and, therefore, finally simplifies the equations.

Anyons and hole live in two different parallel planes separated by the distance h. Nevertheless, only the 2D coordinates of Eq. (1) enter into the exciton wave function. The separation h enters only into the Hamiltonian of the anyon-hole interaction derived in the Sec. III C.

The most general form of the pseudo-wave-function of an anyon exciton meeting all general requirements is as follows:

$$\Psi_{L,\mathbf{k}}(\mathbf{R},\boldsymbol{\rho},\{\overline{z_{jl}}\})=\exp\left\{i\mathbf{k}\mathbf{R}+\frac{i}{2}\hat{z}\cdot(\boldsymbol{\rho}\times\mathbf{R})-\frac{1}{4}(\boldsymbol{\rho}-\mathbf{d})^2\right\}\times P_L(\cdots\overline{z_{jl}}\cdots)\times\prod_{jl}(\overline{z_{jl}})^{\alpha}\exp\{-|z_{jl}|^2/36\}\Big/\sqrt{2\pi A}, \tag{3}$$

where the pair of indices jl takes the values specified in Eq. (1), A is the normalization area, and P_L is a homogeneous polynomial in coordinates $\overline{z_{jl}}$ of the degree L.

The basic properties of the functions $\Psi_{L,\mathbf{k}}$ can be checked by inspection. (i) Since the exciton is a neutral entity, it possesses an in-plane momentum $\mathbf{k}$,[23] and $\Psi_{L,\mathbf{k}}$ satisfies the equation of magnetic translations:

$$T_{\mathbf{a}}\Psi_{L,\mathbf{k}}(\mathbf{R},\boldsymbol{\rho},\{\overline{z_{jl}}\})=\exp[i\mathbf{a}\cdot\mathbf{A}(\boldsymbol{\rho})]\Psi_{L,\mathbf{k}}(\mathbf{R}-\mathbf{a},\boldsymbol{\rho},\{\overline{z_{jl}}\})=e^{-i\mathbf{k}\cdot\mathbf{a}}\Psi_{L,\mathbf{k}}(\mathbf{R},\boldsymbol{\rho},\{\overline{z_{jl}}\}). \tag{4}$$

The parameter $\mathbf{d}=\hat{z}\times\mathbf{k}$ is related to the dipole moment of the exciton $(-\mathbf{d})$. (ii) The function $\Psi_{L,\mathbf{k}}$ belongs to the lowest Landau level. Indeed, the nonanalytic factor of it can be shown to have the form

$$\exp\left\{-\frac{1}{12}\Sigma_j|z_j|^2-\frac{1}{4}|z_h|^2\right\},$$

whereas the other factors are analytic functions of $\overline{z_j}$ and z_h. (iii) The function $P_L(\cdots\overline{z_{jl}}\cdots)$ is a homogeneous polynomial of the degree L which is symmetric in all coordinates $\overline{z_j}$. These polynomials form a boson basis, and the effect of the fractional statistics is taken into account by the factor $\Pi_{jl}(\overline{z_{jl}})^{\alpha}$.[3,31] (iv) A system of four charged particles in a magnetic field possesses four quantum numbers. Two of them are absorbed in the 2D momentum $\mathbf{k}$. Two others determine the form of the polynomial P_L and are internal quantum numbers of an anyon exciton. The operator $\hat{L}_z$ of the z projection of the angular momentum commutes with the Hamiltonian and the square of the momentum, $\hat{\mathbf{k}}^2$, but it does not commute with the projections of $\hat{\mathbf{k}}$, i.e., with $\hat{k}_x$ and $\hat{k}_y$. Therefore, the function $\Psi_{L,\mathbf{k}}$ chosen in the $\hat{k}_x,\hat{k}_y$ representation is simultaneously an eigenfunction of $\hat{L}_z$ only for $\mathbf{k}=0$, and in this limit $L_z=-L$.

Therefore, the quantum numbers of an anyon exciton include the 2D momentum $\mathbf{k}$ and the projection of the angular momentum, $L_z=-L$, of the exciton with $\mathbf{k}=0$. The angular momentum L numerates branches of the exciton spectrum. The fourth quantum number, which will be specified in what follows, numerates branches with coinciding values of L. The multiple-branch structure of the anyon exciton spectrum is a direct consequence of the charge fractionalization which results in the appearance of the internal degrees of freedom of an anyon exciton and of the related internal quantum numbers.

By definition, the polynomial P_L is symmetric in coordinates $\overline{z_j}$. To establish the symmetry of it in the symmetric coordinates $\overline{z_{jl}}$, one can start with a monomial $\overline{z}_{12}^{l_3}\overline{z}_{23}^{l_1}\overline{z}_{31}^{l_2}$, apply to it all operations of the permutation group, and take the sum over the group. This transformation results in the polynomial

$$(\overline{z}_{12}^{l_3}\overline{z}_{23}^{l_1}\overline{z}_{31}^{l_2}+\overline{z}_{23}^{l_3}\overline{z}_{31}^{l_1}\overline{z}_{12}^{l_2}+\overline{z}_{31}^{l_3}\overline{z}_{12}^{l_1}\overline{z}_{23}^{l_2})+(-)^{l_1+l_2+l_3}(\overline{z}_{12}^{l_3}\overline{z}_{31}^{l_1}\overline{z}_{23}^{l_2}+\overline{z}_{23}^{l_3}\overline{z}_{12}^{l_1}\overline{z}_{31}^{l_2}+\overline{z}_{31}^{l_3}\overline{z}_{23}^{l_1}\overline{z}_{12}^{l_2}),$$

which has different properties depending on the parity of $L=l_1+l_2+l_3$. If L is even, the polynomial is a permanent, and, therefore, is symmetric in the coordinates $\overline{z_{jl}}$. However, when L is odd, the polynomial is a determinant which is obviously antisymmetric in the coordinates $\overline{z_{jl}}$ and is nonequal to zero only for $l_1\neq l_2\neq l_3$. For example, for the lowest possible value of L, $L=3$, this determinant turns into a Vandermonde determinant

$$W(\overline{z_{12}},\overline{z_{23}},\overline{z_{31}})=\begin{vmatrix}1 & 1 & 1\\ \overline{z_{12}} & \overline{z_{23}} & \overline{z_{31}}\\ \overline{z}_{12}^{2} & \overline{z}_{23}^{2} & \overline{z}_{31}^{2}\end{vmatrix}=(\overline{z_{12}}-\overline{z_{23}})(\overline{z_{23}}-\overline{z_{31}})(\overline{z_{31}}-\overline{z_{12}}). \tag{5}$$

Therefore, L-even and L-odd polynomials P_L have rather different properties. All of them are symmetric in bosonic permutations $\overline{z_1}\leftrightarrow\overline{z_2}$, etc., but they have opposite symmetry with respect to the permutations of the $\overline{z_{12}}\leftrightarrow\overline{z_{23}}$ type. To find the explicit form of the polynomials P_L, it is convenient to introduce new real coordinates

$$\boldsymbol{\xi}_j=\mathbf{r}_j-\mathbf{r}_0,\quad \mathbf{r}_0=\frac{1}{3}\sum_{l=1}^{3}\mathbf{r}_{jl}, \tag{6}$$

where $\mathbf{r}_0$ is the center of mass of the anyon sybsystem. The corresponding complex coordinates are $\zeta_j=\xi_{jx}+i\xi_{jy}$. These coordinates are subject to the constraint

$$\sum_{j=1}^{3}\boldsymbol{\xi}_j=0,\quad \sum_{j=1}^{3}\zeta_j=0. \tag{7}$$

In these coordinates the bosonic symmetry of P_L has the usual form, and we can apply the fundamental theorem of the theory of symmetric polynomials.[32] According to it, $P_L(\zeta_1,\zeta_2,\zeta_3)$ can be expressed in the unique way as a polynomial in the three elementary symmetric polynomials:

$$p_1=\overline{\zeta_1}+\overline{\zeta_2}+\overline{\zeta_3},\quad p_2=\overline{\zeta_1\zeta_2}+\overline{\zeta_2\zeta_3}+\overline{\zeta_3\zeta_1},\quad p_3=\overline{\zeta_1\zeta_2\zeta_3}. \tag{8}$$

The first polynomial is equal to zero, $p_1=0$, because of the constraint of Eq. (7). Therefore, the polynomials P_L are polynomials only in p_2 and p_3. The first L-even polynomials are $P_0=\text{const}$, $P_2\propto p_2$, $P_4\propto p_2^2$; i.e., there exists only a single elementary polynomial of a given degree L. However, two elementary polynomials, p_2^3 and p_3^2, contribute to P_6. It is easy to check that the number of basis functions increases by one each time when L takes values $L=6m$, where m is an integer. Therefore, the number of L-even polynomials is equal to $[L/6]+1$, where $[L/6]$ is the integral part of $L/6$. All L-odd polynomials can be obtained by multiplying L-even polynomials by p_3. The latter equals $p_3=-\frac{1}{27}W$ because of Eq. (6).

We are now in position to choose a full basis of polynomials P_L in symmetric coordinates $\overline{z_{jl}}$. These coordinates are most convenient for all the following calculations. L-even polynomials can be chosen as

$$P_{L,M}=\overline{z}_{12}^{\,L-4M}\overline{z}_{23}^{\,2M}\overline{z}_{31}^{\,2M}+\overline{z}_{23}^{\,L-4M}\overline{z}_{31}^{\,2M}\overline{z}_{12}^{\,2M}+\overline{z}_{31}^{\,L-4M}\overline{z}_{12}^{\,2M}\overline{z}_{23}^{\,2M}, \tag{9}$$

where $M=0,1,\ldots[L/6]$. Polynomials $P_{L,M}$ are linearly independent, and the total number of polynomials with a given L is equal to $[L/6]+1$. All linearly independent L-odd polynomials can be obtained as

$$P_{L,M}=WP_{L-3,M},\quad P_{3,0}=W. \tag{10}$$

The total number of them equals $[(L-3)/6]+1$.

This choice of polynomials determines the full set of quantum numbers in the wave function of Eq. (3) as L, M, and $\mathbf{k}$. To our best knowledge, in the previous studies only the L-even polynomials have been taken into account.[33] When choosing polynomials $P_{L,M}$, we have not imposed the hard-core constraint and defer the discussion of the related properties to what follows.

It is an important feature of the AEM that the wave functions (and, therefore, electron densities, etc.) of all eigenstates with $L\leqslant 5$ and also $L=7$ are completely determined by the symmetry requirements. They do not depend on the specific form of the Hamiltonian and, in particular, on h.

III. THE SCHRÖDINGER EQUATION

In this section we calculate the Hamiltonian of the AEM in the $\Psi_{L,M,\mathbf{k}}$ basis as the matrix of a point charge Coulomb interaction. It means that we neglect form factors of quasielectrons which have a scale of several magnetic lengths and are known only approximately.[34–36] We postpone the discussion of inaccuracy originating from this approximation to Sec. VII.

Unfortunately, functions $\Psi_{L,M,\mathbf{k}}$ are orthogonal only in quantum numbers L and $\mathbf{k}$. As a result, the scalar products $\langle\Psi_{L,M,\mathbf{k}},\Psi_{L,M',\mathbf{k}}\rangle\neq 0$ for $M\neq M'$, and the matrix $\hat{B}$ of these scalar products is block diagonal. The size of blocks is equal to 1 for $L<6$ and $L=7$ and increases by 1 each time when L increases by 6. With a nondiagonal matrix $\hat{B}$ the Schröedinger equation has a form

$$\hat{H}\chi=\varepsilon\hat{B}\chi, \tag{11}$$

and one has to find matrices $\hat{H}$ and $\hat{B}$. To perform the calculations, it is convenient to employ variables $\mathbf{R}$, $\boldsymbol{\rho}$, and three $\mathbf{r}_{ij}$ and to take into account the constraint of Eq. (2) by the usual transformation:

$$\delta(\mathbf{r}_{12}+\mathbf{r}_{23}+\mathbf{r}_{31})=\int\frac{d\mathbf{f}}{(2\pi)^2}\exp\{i\mathbf{f}\cdot(\mathbf{r}_{12}+\mathbf{r}_{23}+\mathbf{r}_{31})\}. \tag{12}$$

It adds the new variable $\mathbf{f}$, but all calculations become symmetric in anyon variables. The Jacobian of the transformation is equal to 1.

The Hamiltonian is diagonal in $\mathbf{k}$; therefore, we write out only the diagonal in $\mathbf{k}$ matrix elements. For $\mathbf{k}=0$, the Hamiltonian is also diagonal in L, and Eq. (11) acquires a block diagonal form.

Since all terms in the polynomials $P_{L,M,\mathbf{k}}$, Eqs. (9) and (10), have the same form, we concentrate in what follows on the matrix elements taken in the basis of the functions $\Psi_{\{n\}\mathbf{k}}$:

$$\Psi_{\{n\}\mathbf{k}}(\mathbf{R},\boldsymbol{\rho},\{\overline{z_{jl}}\})=\exp\left\{i\mathbf{k}\mathbf{R}+\frac{i}{2}\hat{z}\cdot(\boldsymbol{\rho}\times\mathbf{R})-\tfrac{1}{4}(\boldsymbol{\rho}-\mathbf{d})^2\right\}\overline{z}_{12}^{\,n_3+\alpha}\overline{z}_{23}^{\,n_1+\alpha}\overline{z}_{31}^{\,n_2+\alpha}\times\exp\left\{-\sum_{jl}|z_{jl}|^2/36\right\}\Big/\sqrt{2\pi A}. \tag{13}$$

Here polynomials $P_{L,M}$ are substituted by monomials, and $\{n\}$ denotes a set of quantum numbers n_1, n_2, and n_3. In the following parts of this section we describe in some detail the technique for performing different types of integrals.

A. Nonorthogonality matrix elements

The scalar products of functions $\Psi_{\{n\}\mathbf{k}}$, when written in the variables $\mathbf{R}$, $\boldsymbol{\rho}$, and $\mathbf{r}_{jl}$, have the form

$$B_{\{n\}\{n'\}}=\langle\{n\}|\{n'\}\rangle=\int d\mathbf{R}\int d\boldsymbol{\rho}\int\frac{d\mathbf{f}}{(2\pi)^2}\int d\mathbf{r}_{12}d\mathbf{r}_{23}d\mathbf{r}_{31}\overline{\Psi}_{\{n\}\mathbf{k}}\times\Psi_{\{n'\}\mathbf{k}}\exp\{i\mathbf{f}\cdot(\mathbf{r}_{12}+\mathbf{r}_{23}+\mathbf{r}_{32})\}. \tag{14}$$

Integration over $\mathbf{R}$ and the Gaussian integration over $\boldsymbol{\rho}$ are straightforward. Since $\Psi_{\{n\}\mathbf{k}}$ is multiplicative in the variables $\mathbf{r}_{jl}$, one can rewrite Eq. (14) in the form

$$\langle\{n\}|\{n'\}\rangle=\int \frac{d\mathbf{f}}{(2\pi)^2}\prod_{j=1}^{3} M^{(\alpha)}_{n_j n'_j}(\mathbf{f}), \tag{15}$$

where

$$M^{(\alpha)}_{mm'}(\mathbf{f})=\int d\mathbf{r}\; r^{2\alpha} z^m \overline{z}^{\,m'} e^{-r^2/18+i\mathbf{f}\cdot\mathbf{r}}. \tag{16}$$

Since

$$\int_0^{2\pi} d\varphi e^{\pm im\varphi+ifr\cos\varphi}=2\pi i^{|m|}J_{|m|}(fr), \tag{17}$$

where $J_{|m|}(fr)$ is a Bessel function, the angle integration in Eq. (16) results in

$$M^{(\alpha)}_{mm'}(\mathbf{f})=2\pi i^{|m-m'|}\exp[i(m-m')\varphi_{\mathbf{f}}]\mathcal{M}^{(\alpha)}_{mm'}(t), \tag{18}$$

where $t=9f^2/2$, $\varphi_{\mathbf{f}}$ is the azimuth of $\mathbf{f}$, and

$$\mathcal{M}^{(\alpha)}_{mm'}(t)=\int_0^{\infty} dr r^{1+2\alpha+m+m'} e^{-r^2/18} J_{|m-m'|}(fr). \tag{19}$$

This integral can be expressed in terms of the confluent hypergeometric function $\Phi(\beta,\gamma;t)$ as[37]

$$\begin{aligned}\mathcal{M}^{(\alpha)}_{mm'}(t)=&\Gamma(\max\{m,m'\}+\alpha+1)\\ &\times\frac{2^{|m+m'|/2+\alpha}3^{|m+m'|+2(\alpha+1)}}{|m-m'|!}t^{|m-m'|/2}\\ &\times\Phi(\max\{m,m'\}+\alpha+1,|m-m'|+1;-t).\end{aligned} \tag{20}$$

Here $\max\{m,m'\}$ is the larger of the integers m and m'. After the integration over $\varphi_{\mathbf{f}}$ in Eq. (15), the coefficients $\langle\{n\}|\{n'\}\rangle$ take the form

$$\langle\{n\}|\{n'\}\rangle=\delta_{nn'}(2\pi/3)^2\int_0^{\infty} dt\prod_{j=1}^{3} i^{|n_j-n'_j|}\mathcal{M}^{(\alpha)}_{n_j n'_j}(t), \tag{21}$$

where

$$n=n_1+n_2+n_3. \tag{22}$$

Therefore, the scalar product $\langle\{n\}|\{n'\}\rangle$ of two functions $\Psi_{\{n\}\mathbf{k}}$ is reduced to a onefold integral from the product of three confluent hypergeometric functions. Matrix elements $\langle\{n\}|\{n'\}\rangle$ do not depend on $\mathbf{k}$. Scalar products $\langle L,M|L',M'\rangle$ of two functions $\Psi_{L,M,\mathbf{k}}$, which include polynomials $P_{L,M}$, are linear combinations of the coefficients $\langle\{n\}|\{n'\}\rangle$. They do not depend on $\mathbf{k}$ either. The coefficients of these combinations can be found from Eqs. (5), (9), and (10), but the final expressions are rather cumbersome, especially for L-odd polynomials. Therefore, we do not write out here their explicit form.

Integrals (21) can be simplified for $\alpha=0$. Indeed, in this case the Kummer transformation[37]

$$\Phi(\beta,\gamma;t)=e^t\Phi(\gamma-\beta,\gamma;-t) \tag{23}$$

results in a Φ function with the first parameter $(\gamma-\beta)$ equal to a negative integer. This function reduces to a polynomial, and $\Phi(\beta,\gamma;t)$ to a polynomial multiplied by e^t. Therefore, the integral in Eq. (21) for $\langle\{n\}|\{n'\}\rangle$ can be performed exactly. This transformation highly simplifies calculations. Indeed, in the large h region, where the criterion of the applicability of the AEM is satisfied, the statistical parameter α can be neglected as it is shown in Sec. IV below.

B. Anyon-anyon interaction

The Hamiltonian of the anyon-anyon interaction is

$$\hat{V}_{aa}=\tfrac{1}{9}\{|\overline{z_{12}}|^{-1}+|\overline{z_{23}}|^{-1}+|\overline{z_{31}}|^{-1}\}. \tag{24}$$

Matrix elements of $\hat{V}_{aa}$ in the basis of the functions $\Psi_{\{n\}\mathbf{k}}$ can be calculated by analogy with the matrix elements $\langle\{n\}|\{n'\}\rangle$. The denominators $|\overline{z_{jl}}|^{-1}$ lower the power of r by 1 in one of the $\mathcal{M}^{(\alpha)}_{n_j n'_j}(\mathbf{f})$ factors entering in Eq. (15). The final expression for the matrix element is

$$\begin{aligned}&\langle\{n\}|\hat{V}_{aa}|\{n'\}\rangle\\ &=\frac{1}{9}\int\frac{d\mathbf{f}}{(2\pi)^2}\Big\{M^{(\alpha-1/2)}_{n_1 n'_1}(\mathbf{f})M^{(\alpha)}_{n_2 n'_2}(\mathbf{f})M^{(\alpha)}_{n_3 n'_3}(\mathbf{f})\\ &\quad+M^{(\alpha)}_{n_1 n'_1}(\mathbf{f})M^{(\alpha-1/2)}_{n_2 n'_2}(\mathbf{f})M^{(\alpha)}_{n_3 n'_3}(\mathbf{f})\\ &\quad+M^{(\alpha)}_{n_1 n'_1}(\mathbf{f})M^{(\alpha)}_{n_2 n'_2}(\mathbf{f})M^{(\alpha-1/2)}_{n_3 n'_3}(\mathbf{f})\Big\}.\end{aligned} \tag{25}$$

Like the nonorthogonality matrix elements, matrix elements of $\hat{V}_{aa}$ also do not depend on the momentum $\mathbf{k}$. For this reason, the matrix of the operator $\hat{V}_{aa}$ is diagonal in the angular momentum, L, for arbitrary values of the momentum $\mathbf{k}$.

C. Anyon-hole interaction

The Hamiltonian of the anyon-hole interaction has a form

$$\hat{V}_{ah}=-\frac{1}{3}\sum_{j=1}^{3}\hat{V}_{jh},\quad \hat{V}_{jh}(\mathbf{r}_{jh})=r_{jh}^{-1}, \tag{26}$$

where the three-dimensional anyone-hole separation $\mathbf{r}_{1h}$ should be expressed in terms of the difference coordinates:

$$\mathbf{r}_{1h}=\boldsymbol{\rho}+\tfrac{1}{3}(\mathbf{r}_{12}-\mathbf{r}_{31})+\hat{z}h. \tag{27}$$

Similar equations hold for $\mathbf{r}_{2h}$ and $\mathbf{r}_{3h}$.

It is convenient to introduce the Fourier image

$$\hat{V}_{1h}(\mathbf{r}_{1h}) = -\frac{1}{3}\int \frac{d\mathbf{q}}{(2\pi)^2} V_{ah}(q) \times \exp\left\{ i\mathbf{q}\cdot\boldsymbol{\rho} + \frac{i}{3}\mathbf{q}\cdot(\mathbf{r}_{12}-\mathbf{r}_{31})\right\}, \qquad (28)$$

where $V_{ah}(q) = (2\pi/q)\exp(-qh)$. The integrations over $\mathbf{R}$ and $\boldsymbol{\rho}$ in the matrix elements of $\hat{V}_{1h}(\mathbf{r}_{1h})$ can be performed in the same way as in Eq. (14), and the result can be expressed in terms of the coefficients $M^{(\alpha)}_{mm'}$, Eq. (16), as

$$\langle\{n\}|\hat{V}_{1h}|\{n'\}\rangle = -\frac{1}{3}\int \frac{d\mathbf{f}}{(2\pi)^2}\int \frac{d\mathbf{q}}{(2\pi)^2} V_{ah}(q) e^{-q^2/2 + i\mathbf{k}\cdot\mathbf{q}} \times M^{(\alpha)}_{n_1 n_1'}(\mathbf{f}) M^{(\alpha)}_{n_2 n_2'}(\mathbf{f}-\mathbf{q}/3) M^{(\alpha)}_{n_3 n_3'}(\mathbf{f}+\mathbf{q}/3). \qquad (29)$$

After the angular integration, the factors $M^{(\alpha)}_{n_j n_j'}$ take the form of Eq. (18), and Eq. (29) can be rewritten as

$$\langle\{n\}|\hat{V}_{1h}|\{n'\}\rangle = -\frac{(2\pi)^2}{3}\prod_{j=1}^{3} i^{|n_j-n_j'|}\int \frac{d\mathbf{f}}{(2\pi)^2}\int \frac{d\mathbf{q}}{(2\pi)^2} V_{ah}(q) e^{-q^2/2 + i\mathbf{k}\cdot\mathbf{q}} \exp\{ i\varphi_{\mathbf{f}}(n_1-n_1') + i\varphi_-(n_2-n_2') + i\varphi_+(n_3-n_3')\} \mathcal{M}^{(\alpha)}_{n_1 n_1'}(9f^2/2) \mathcal{M}^{(\alpha)}_{n_2 n_2'}(9f_+^2/2) \mathcal{M}^{(\alpha)}_{n_3 n_3'}(9f_-^2/2). \qquad (30)$$

Vectors $\mathbf{f}_\pm$ are defined by the equation

$$\mathbf{f}_\pm = \mathbf{f} \pm \mathbf{q}/3. \qquad (31)$$

One can perform one angular integration in Eq. (30) if the phase $\varphi_{\mathbf{f}}$ is eliminated by change in the variables:

$$\varphi = \varphi_{\mathbf{f}} - \varphi_{\mathbf{q}}, \quad \psi_\pm = \varphi_\pm - \varphi_{\mathbf{f}}. \qquad (32)$$

Here $\varphi_\pm$ are phases of vectors $\mathbf{f}_\pm$.

After the integration over $\varphi_{\mathbf{q}}$, Eq. (29) takes its final form:

$$\langle\{n\}|\hat{V}_{1h}|\{n'\}\rangle = -\frac{1}{3} i^{|n-n'|}\prod_{j=1}^{3} i^{|n_j-n_j'|}\int_0^\infty df f \int_0^\infty dq q V_{ah}(q) e^{-q^2/2} J_{|n-n'|}(kq) \int_0^{2\pi} d\varphi \exp\{ i\varphi(n-n') + i\psi_-(n_2-n_2') + i\psi_+(n_3-n_3')\} \mathcal{M}^{(\alpha)}_{n_1 n_1'}(9f^2/2) \mathcal{M}^{(\alpha)}_{n_2 n_2'}(9f_+^2/2) \mathcal{M}^{(\alpha)}_{n_3 n_3'}(9f_-^2/2). \qquad (33)$$

Here the direction of $\mathbf{k}$ was chosen along the x axis to eliminate the complex phase from the matrix element (33). Explicit expressions of $\psi_\pm$ and $f_\pm$ in terms of the integration variables are as follows:

$$e^{i\psi_\pm} = \left(f \pm \frac{q}{3} e^{-i\varphi}\right) \Big/ f_\pm, \quad f_\pm^2 = f^2 + (q/3)^2 \pm \frac{2}{3} fq\cos\varphi. \qquad (34)$$

One can check by inspection that Eq. (33) is symmetric in the indices n_2, n_2' and n_3, n_3', and that matrix elements are real for all sets of the quantum numbers $\{n_j\},\{n_j'\}$ compatible with our choice of the polynomials $P_{L,M}$, Eqs. (9) and (10). Matrix elements of the operators $\hat{V}_{2h}$ and $\hat{V}_{3h}$ can be written by analogy with Eq. (33).

Equations (25) and (33) for the Hamiltonian $\hat{H}$ and Eqs. (14) and (21) for the matrix $\hat{B}$ determine completely the Schrödinger equation (11).

IV. ENERGY SPECTRUM

For $\mathbf{k}=0$ the operator of the anyon-hole interaction $\hat{V}_{ah}$ becomes diagonal in the angular momentum L. Therefore, the Schrödinger equation (11) is also diagonal in L since $\hat{V}_{aa}$ and $\hat{B}$ are diagonal in L for arbitrary $\mathbf{k}$. It was shown in Sec. II that for each value of L such that $L \leqslant 5$ or $L=7$ there exists a single eigenfunction, and it does not depend on h. For these values of L the equations of Sec. III immediately give the energies of $\mathbf{k}=0$ states. When the number of $P_{L,M}$ polynomials with a given value of L becomes two or more, equations of Sec. III give the coefficients of secular equations of the second, third, etc., order which determine the h dependent eigenfunctions and eigenvalues.

The order in which $\mathbf{k}=0$ levels are arranged changes with increasing h. The main regularities can be understood using classical arguments. In the classical limit, which is achieved for a large exciton size, the exciton ground state takes the shape of an equilateral triangle with anyons in the vertices and a hole in the center. The anyon-anyon distance in this triangle, r_{12}, found from the minimum of the electrostatic energy, is equal to

$$r_{12} = \sqrt{3/2}h. \qquad (35)$$

It will be shown below that triangular configurations are described by the polynomials $P_{6M,M}$ and $WP_{6M,M}$. A straightforward calculation based on Eqs. (3), (9), and (10) shows that a mean-square value of the interanyon distance in these states is equal to

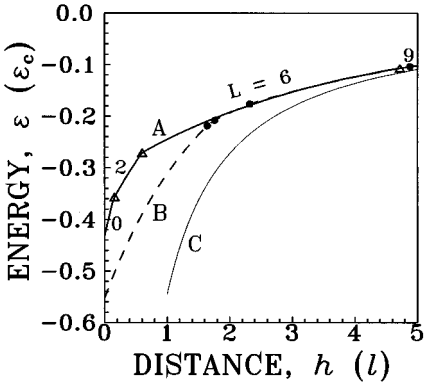

FIG. 1. Ground-state energy, $\varepsilon(\mathbf{k}=0)$, plotted versus separation h between electron and hole confinement planes. A and B — statistical charges $\alpha=-1/3$ and $\alpha=0$, respectively. A — triangles show the points where the angular momentum L changes from zero to 2, and then to 6 and 9. For the quantum states separated by full dots on curve B see Fig. 4. C — classical limit.

$$\langle r_{12}^2\rangle = 6(L+2+3\alpha). \tag{36}$$

Comparing Eqs. (35) and (36) one finds that

$$r_{12}\sim h\sim L^{1/2} \tag{37}$$

for $L\gg 1$. Therefore, with increasing h both the size r_{12} and the angular momentum L of the exciton ground state increase. This means that the order of the energy levels changes, and the bottom state possesses the angular momentum $L\sim h^2$. Since for $\mathbf{k}=0$ the Hamiltonian is diagonal in L, the level interchange occurs usually as a level crossing.

In Fig. 1 the ground-state energy is plotted as a function of h for two values of the statistical charge, $\alpha=-1/3$ and $\alpha=0$, by curves A and B, respectively. It is seen that both curves show the same gross features, including increase of the ground-state energy and the angular momentum with h. However, fine details are very different in the $h<2$ region. We do not discuss these differences in more detail since they are expected to be sensitive to anyon form factors,[34–36] which were not taken into account in our calculations. However, since curves A and B practically coincide for $h\gtrsim 2$, we believe that in this region the AEM provides reliable results. In what follows we restrict ourselves to this region and neglect the statistical charge, i.e., consider the bosonic model, $\alpha=0$. All data below are presented for this model. It was shown in Sec. III A, Eq. (23), that for $\alpha=0$ matrix elements $\mathcal{M}^{(\alpha)}_{mm'}(t)$ can be expressed in terms of elementary functions. This fact permits one to reduce the threefold integral of Eq. (33) to the onefold integral:

$$\langle LM\mathbf{k}|V_{ah}|L'M'\mathbf{k}\rangle = -\int_0^\infty \exp(-3q^2/2-qh)J_{|L-L'|}(kq)Q_{LM,L'M'}(q)dq, \tag{38}$$

where functions $Q_{LM,L'M'}(q)$, real and symmetric in indices, are polynomials in q. The lower polynomials are of a simple form: $Q_{00,00}=1$, $Q_{20,00}=q^2/2$, $Q_{20,20}=1-q^2+q^4/4$. Application of Eq. (38) highly simplifies all computations.

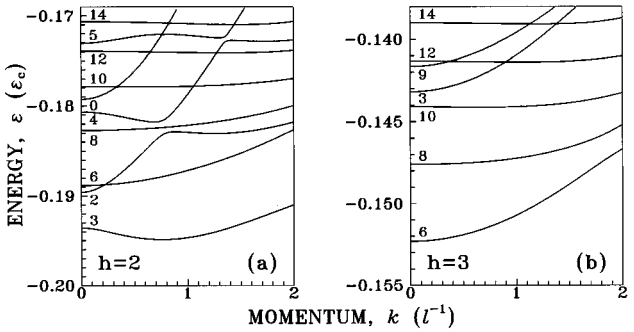

FIG. 2. Anyon exciton dispersion law $\varepsilon(k)$ for two values of h. For $h=2$, the negative dispersion arises because of the mutual repulsion of $L=2$ and $L=3$ branches. Level splitting near avoided crossings becomes tiny with increasing h. Numbers show L values. h in units of l.

For comparison, in Fig. 1 is also shown the energy $\varepsilon_{\rm cl}=-(2/3)^{3/2}/h$ calculated in the classical limit, Eq. (35). It is seen that in the region $h\lesssim 4$ it differs considerably from the exact quantum data.

Since for $\mathbf{k}\neq 0$ the term $\hat{V}_{ah}$ is nondiagonal in L, the dispersion law $\varepsilon(k)$ can be found only numerically. In Fig. 2 it is shown for two values of h. The basis of polynomials used in computations included 22 L-even polynomials with $L\leqslant 18$, Eq. (8), and 22 L-odd polynomials with $L\leqslant 21$, Eq. (9). The following regularities are distinctly seen. As argued above, the levels with higher L values draw closer to the spectrum bottom with increasing h. The level interchange manifests itself as avoided level crossings. The level splitting near these crossings increases with k and decreases with the difference $|L-L'|$. These regularities can be understood if one takes into account that the Bessel function in the integrand of Eq. (38) shows the power-law behavior, $J_{|L-L'|}(kq)\propto(kq)^{|L-L'|}$, in the small k region. In particular, for $|L-L'|=1$ the interaction of two branches can result in the negative exciton effective mass for small k values. Negative exciton dispersion can appear even in the ground state as can be seen in Fig. 2(a). It is interesting to mention that exciton dispersion near $\mathbf{k}=0$ is always positive in the two-semion problem.[11]

The above results show that the charge fractionalization determines both (i) the basic multiple-branch structure of the exciton energy spectrum and (ii) numerous specific features of the spectrum including the h dependence of the arrangement of the branches, avoided branch intersections, etc.

V. ELECTRON DENSITY

The distribution of the electron density, $D_\lambda(\mathbf{r},\mathbf{k})$, around a hole can be found from the equation

$$D_\lambda(\mathbf{r},\mathbf{k}) = \left\langle \frac{1}{3}\sum_{j=1}^{3}\delta(\mathbf{r}_j-\mathbf{r}_h-\mathbf{r})\right\rangle_{\lambda\mathbf{k}}, \tag{39}$$

where the averaging is performed over the quantum state $(\lambda,\mathbf{k})$, where λ numerates exciton branches. The density $D_\lambda(\mathbf{r},\mathbf{k})$ is exactly the quantity which (i) permits one to check reliability of the model and in which (ii) the specific

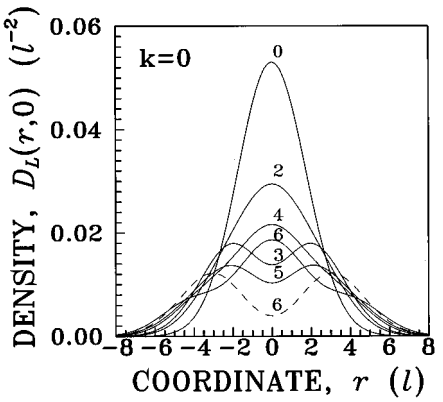

FIG. 3. Axisymmetric electron density distributions $D_L(r,0)$ for a $\mathbf{k}=0$ exciton for the states with $L\leqslant 6$. Two $L=6$ states are shown for $h=0$; the density distribution in the lower state is shown by a solid line. Numbers show L values.

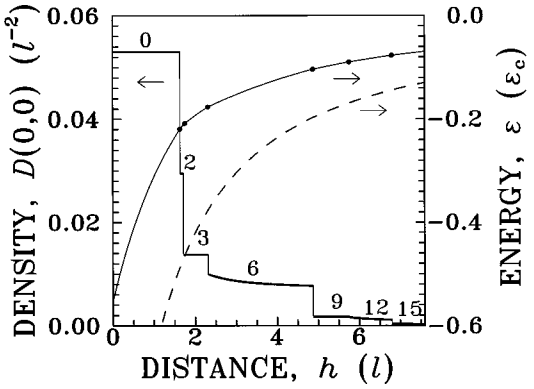

FIG. 4. The energy $\varepsilon(0)$ and the electron density $D(0,0)$ at the point $\mathbf{r}_h$ where the hole resides plotted *vs* h for the ground state of an exciton with $k=0$. The ground-state energy of an anyon exciton is shown by a solid line; the dots on it show the positions of the intersections between the energy levels with different L values. For comparison the energy of a conventional magnetoexciton $\varepsilon_{\rm me}(h)$ with $k=0$ is shown by a dashed line. Numbers near the $D(0,0)$ curve show the L values. Only the states with $L=3m$ reach the spectrum bottom (as an exclusion the state $L=2$ appears as a bottom state in an extremely narrow region of the h values).

pattern of the charge fractionalization manifest itself in a rather spectacular way. It is one of the basic criteria of the AEM that the excess charge density is small compared with the density of the IQL, $\nu/2\pi$, for $\nu<1/2$ [and compared with $(1-\nu)/2\pi$ for $\nu>1/2$]. Therefore, for $\nu=1/3$ and $\nu=2/3$ IQL's one can expect that the AEM becomes applicable only when $D_\lambda \ll 1/6\pi \approx 0.05$. This criterion will be applied in what follows.

The explicit expression for D_λ can be obtained in the same way as Eq. (38). Indeed, the operator $\hat{V}_{ah}$ and the operator of the electron density of Eq. (39) depend on the same arguments, $\mathbf{r}_j-\mathbf{r}_h$. Therefore, the integrands differ only in the substitution $V_{ah}(q)$ by the Fourier image of $\delta(\mathbf{r}_j-\mathbf{r}_h)$. The final expression is

$$D_\lambda(\mathbf{r},\mathbf{k})=\frac{1}{2\pi}\sum_{LM,L'M'}\cos[(L-L')\theta]\times\int_0^\infty dqq \times\exp(-3q^2/2)J_{|L-L'|}(q|\mathbf{r}-\mathbf{d}|) \times Q_{LM,L'M'}(q)\overline{\chi}^{\lambda}_{L'M'}(\mathbf{k})\chi^{\lambda}_{LM}(\mathbf{k}), \qquad (40)$$

where θ is the angle between the vectors $\mathbf{d}-\mathbf{r}$ and $\mathbf{d}$. $D_\lambda(0,\mathbf{k})$ shows the electron density on the hole.

For $\mathbf{k}=0$, the density distribution $D_\lambda(r,0)$ is shown in Fig. 3 for $L\leqslant 6$. In this case λ can be completely identified by the index L for $L\leqslant 5$, but there are two functions for $L=6$. For $L\leqslant 5$ the energies, the eigenfunctions, and therefore also the densities D_L, do not depend on h. The $L=0$ state has a high density; $D_0(0,0)>0.05$. Therefore, the shape of the curve $D_0(r,0)$ cannot be reliable. Nevertheless, it is remarkable that numerical calculations performed in the spherical geometry for $\nu=1/3$ (Refs. 12, 16, 25, 38) and $\nu=2/3$ IQL's (Refs. 17) convincingly show that for $h\lesssim 2$ the spectrum bottom is made by the $L=0$ exciton having the electron density which is very close to the Fermi limit, $1/2\pi$.[16,20] Functions $D_{L,M}$ become broader with increasing L, and $D_{L,M}(0,0)$ decreases. The state $L=3$ from which L-odd polynomials originate is especially remarkable because it is the first to show a craterlike density distribution with a minimum at $r=0$. This minimum is a signature of the charge fractionalization, since for ordinary magnetoexcitons the density shows a maximum at $r=0$. We will discuss the properties of this state in more detail in Sec. VI. For $L=6$ there are two eigenfunctions; they depend on h. In Fig. 3 they are shown for $h=0$; the lower-energy component is drawn by a solid line.

Figure 4 shows the energy $\varepsilon(0)$ and the density $D(0,0)$ for bottom states as a function of h. It is seen from the figure that for $h\gtrsim 2$ the density falls well below its critical value 0.05, which supports our above conjecture, Sec. IV, that the AEM provides reliable results for $h\gtrsim 2$. With increasing h the angular momentum in the bottom state, L, also increases. It is a striking feature of the data that only states with $L=3n$, $n\geqslant 2$, reach the spectrum bottom (we cannot make definite conclusions about the $L=3$ state since it does nor reach the bottom for $\alpha=-1/3$ anyons, Fig. 1). The bottom states described by L-even and L-odd polynomials alternate. We attribute the periodicity in L to the superselection rule originating from the combination of the space and permutation symmetry. Indeed, we observe this periodicity in the semiclassical region where the quantization rule includes angular integration between two exchange points separated by the angle $2\pi/3$ rather than the usual 2π integration.[39]

Polynomials $P_{L,M}$ with $L=6M$ play a special role in the class of L-even polynomials. All of them obey the hard-core constraint. Indeed, the polynomial $P_{6M,M}(\overline{z_{12}},\overline{z_{23}},\overline{z_{31}})$ vanishes as $\overline{z}_{jl}^{L/3}$ each time when one of its arguments, $\overline{z}_{jl}$, turns into zero. From the standpoint of the general theory,[31] hard-core functions are the only ''legitimate'' wave functions of an anyon system. The exponent $L/3$ is the maximum order of the zero for a wave function with the angular momentum L, and this maximum is achieved only for $P_{6M,M}$ polynomials. Therefore, Coulomb repulsion is strongly suppressed for these polynomials. Polynomials $WP_{6M,M}$ play a similar role in the class of L-odd polynomials. It is a remarkable fact that in the $h\gtrsim 2$ region all bottom states are either $P_{6M,M}$ or $WP_{6M,M}$ polynomials.

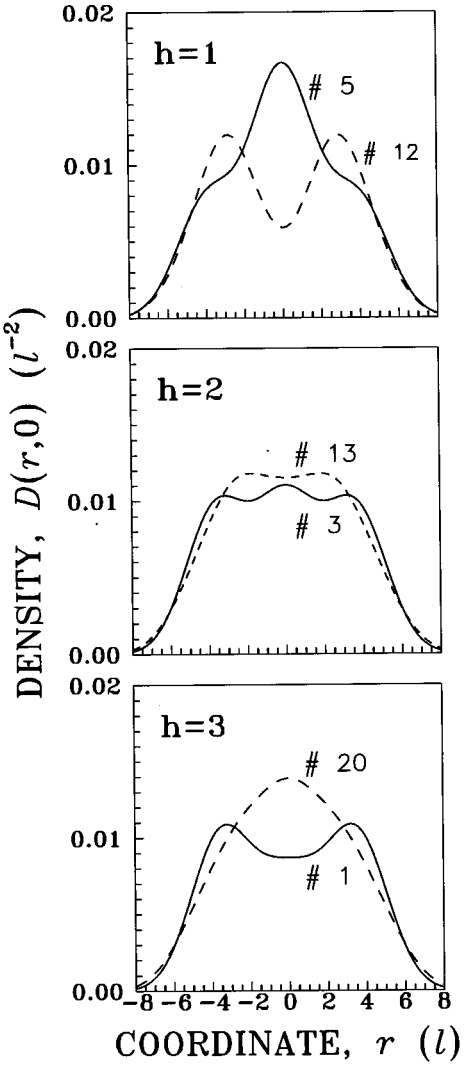

FIG. 5. Electron density distribution $D(r,0)$ for the $L=6$ states with $k=0$ for three values of h. The density in the lower energy state is shown by a solid line. Consecutive numbers, λ, of the energy levels are shown near the curves.

Using the polynomials $P_{6,M}$, $M=0$ and 1, as an example, we can follow the way in which hard-core states move to the spectrum bottom when h increases. For small h values the low-energy component of the $L=6$ doublet has a pronounced maximum near $r=0$ as seen in Figs. 3 and 5. For $h<2$ the low-energy component is close to $\Psi_{6,0}$; for $h=0$ the overlap is 0.96. For $h\approx 2$ wave functions of both components are strongly mixed, and they show similar distributions of the density, Fig. 5. For $h>2$ the function $\Psi_{6,1}$ wins the competition. For $h=3$ it dominates in the low-energy state; the overlap is 0.97. The density $D_{6M,M}(r,0)$ has a single maximum for each value of M. One can obtain a simple analytic expression for the position of the maximum by averaging the density over $\mathbf{r}_h$. This latter function, $\tilde{D}_{L,M}(r,0)$, reaches the maximum at $r_L=\sqrt{2L}$, and the maximum of $D_{L,M}(r,0)$ is very close to this value. More detailed information on the nature of the $\mathbf{k}=0$ bottom states comes from the correlation functions which are discussed in Sec. VI below.

For comparison, in Fig. 4 is also shown the h dependence of the energy of a conventional magnetoexciton, $\varepsilon_{\rm me}(h)$, with the momentum $\mathbf{k}=0$. In the limit $h\to 0$ this energy exactly coincides with the energy of an exciton in the many-electron system because of the hidden symmetry inherent in the problem; see Refs. 14 and 19 and references therein. In the region of $h\ll 1$ the accuracy of the AEM is low. However, it increases for $h\gtrsim 2$ when the charge fractionalization becomes important. In this region $\varepsilon_{\rm me}(h)$ follows the usual Coulomb law, $\varepsilon_{\rm me}(h)\approx -1/h$, whereas for many-electron systems the dependence of the exciton binding energy on h also is close to a Coulomb law, but the numerator is considerably less than 1 since the electron density distribution has a width about h. The magnetoexciton and AEM approaches are exact in the opposite limits. The results should be matched in the intermediate region at $h\approx 2$.

Above in this section we discussed the electron density distribution only for $\mathbf{k}=0$ anyon-excitons. The charge fractionalization manifests itself for these excitons in the crater shape of $D_\lambda(r,0)$. However, the most spectacular manifestation of the charge fractionalization can be expected in the large k region, $k\gtrsim 1$. Indeed, the exciton dipole moment $\mathbf{d}$ differs from $\mathbf{k}$ only by the rotation by $\pi/2$, Sec. II. Therefore, one can expect that with increasing k the electron density splits into bundles, their charges being multiples of 1/3. The splitting of the electron shell into two well separated quasiparticles has been observed previously for a two-semion exciton.[11] For a three-anyon-exciton the patterns are much more impressive. For the bottom state, they are shown in Fig. 6 for $h=3$ when the criterion of the large electron-hole separation is fulfilled. The distribution which is cylindrically symmetric for $k=0$ transforms with increasing k into a distribution with a single split-off anyon ($k=2$ and 3). Two anyons constituting the exciton core show a slight but distinct splitting in a perpendicular direction. This core can be considered as an anyon ion. The core changes its shape with k but remains stable in a wide range of k. Finally, for rather large k values, it splits in the $\mathbf{d}$ direction as it is seen in the last figure, $k=6$. The asymmetric density distribution for $\mathbf{k}\neq 0$ arises completely due to the admixture of L-odd polynomials to the $L=6$ state.

The well-outlined profiles of the electron density seen in Fig. 6 may be smeared by the oscillatory screening inherent in IQL's.[40] Nevertheless, the basic pattern of the charge separation in an exciton should strongly influence the k dependence of the magnetoroton-assisted recombination processes since charge-density excitations are left in a crystal afterwards.

VI. PAIR-CORRELATION FUNCTIONS

One can see in Fig. 3 that the $L=3$ state is the first state which shows a craterlike shape of the density $D(\mathbf{r},0)$. This shape indicates the existence of the anyon substructure of an exciton as it was argued in Sec. V. It is typical of all bottom states with $L\geqslant 6$. In this section we compare properties of $\Psi_{3,0}$ and $\Psi_{6,1}$ states and show that despite the similarity in the shape of the density, they differ critically in the shape of the radial pair-correlation function $w(r)$.

It is convenient to use the square of the wave function Ψ of Eq. (3) averaged over the hole coordinate. Using Eqs.

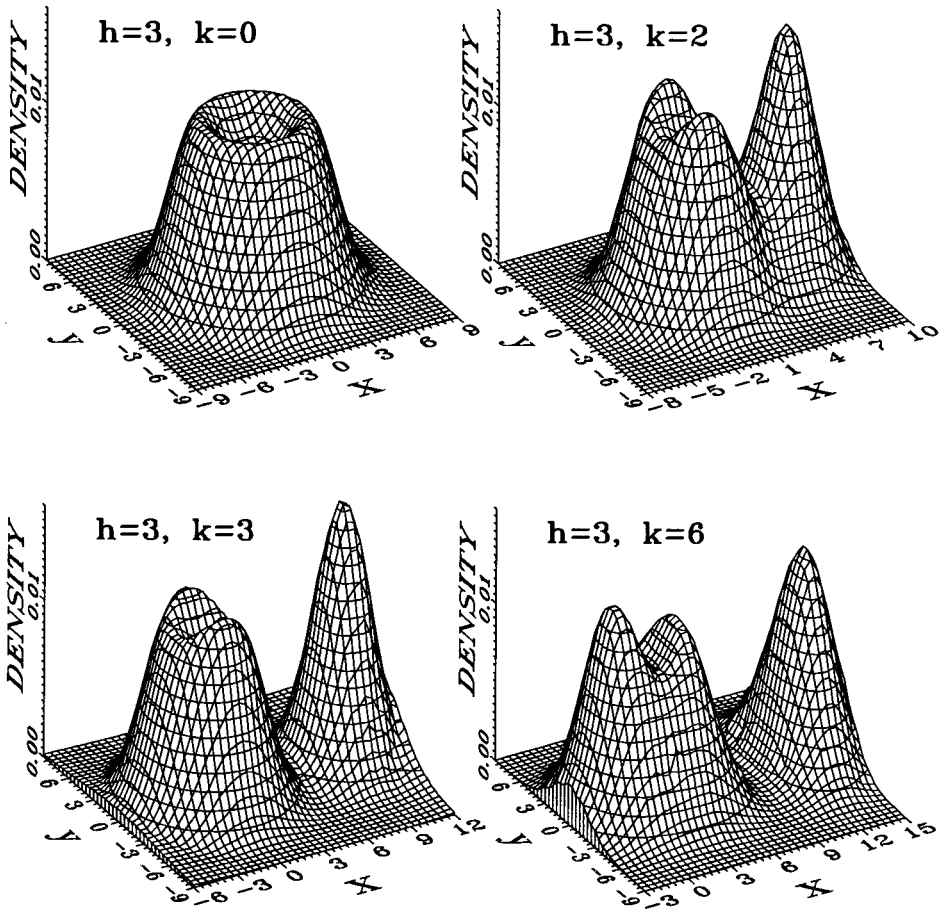

FIG. 6. Electron density distribution in an anyon exciton for different values of k. A hole is at the origin; the x axis is chosen in the **d** direction. The center of the electron density distribution is at $x=k$, y=0. The data were obtained with the 44 polynomial basis, $L\leqslant 21$; data for the 70 polynomial basis, $L\leqslant 27$, also show the change in the shape of the exciton core for large k values. x, y, and h in units of l; k in units of l^{-1}; density in units of l^{-2}.

(3) and (9) and performing Gaussian integration over $\mathbf{r}_h$, one can write the following equation for the averaged $\Psi_{6M,M}$ function:

$$|\widetilde{\Psi}_{6M,M}(\overline{z_{12}},\overline{z_{23}},\overline{z_{31}})|^2\propto(r_{12}r_{23}r_{31})^{4M}\times\exp\left\{-\frac{1}{18}(r_{12}^2+r_{23}^2+r_{31}^2)\right\}. \tag{41}$$

Choosing r_{12}, r_{13}, and ψ, where ψ is the angle between the vectors $\mathbf{r}_{12}$ and $\mathbf{r}_{13}$, as independent variables, rewriting $|\widetilde{\Psi}_{6M,M}|^2$ in terms of these variables, and looking for the maximum first over $\cos\psi$ and then over r_{12} and r_{13}, one finds that the maximum of $|\widetilde{\Psi}_{6M,M}|^2$ is reached for a configuration of an equilateral triangle with

$$r_{12}^2=r_{23}^2=r_{31}^2=6L. \tag{42}$$

In the semiclassical limit, $L\gg 1$, this result coincides with Eq. (36).

To find the most probable configuration for the $\Psi_{3,0}$ state it is convenient to work in ξ variables, Sec. II, and perform averaging over $\mathbf{r}_h$. Simple calculation shows that

$$|\widetilde{\Psi}_{3,0}(\overline{z_{12}},\overline{z_{23}},\overline{z_{31}})|^2\propto\xi_1^2\xi_2^2\xi_3^2\exp\left\{-\frac{1}{6}(\xi_1^2+\xi_2^2+\xi_3^2)\right\}. \tag{43}$$

The maximum of this expression under the constraint of Eq. (7) can be found in the same way as for Eq. (41). Finally, one recovers an equilateral triangle configuration with $r_{12}^2=r_{23}^2=r_{31}^2=18$. This result coincides with Eq. (42) for $L=3$.

Because arbitrary L-odd polynomials have the form $P_{L,M}=WP_{L-3,M}$, Eq. (10), and the equilateral triangle configuration is optimal for each of the multipliers, it is optimal also for their product, $P_{L,M}$. Therefore, the most probable configuration has the same shape of an equilateral triangle both for L-even and L-odd-states.

To reveal a striking difference in the properties of $\Psi_{6,1}$ and $\Psi_{3,0}$ states, one can calculate the radial pair correlation functions $w(r)$:

$$w(r_{12})=\int|\Psi(\mathbf{R},\boldsymbol{\rho},\{\overline{z_{jl}}\})|^2\delta(\mathbf{r}_{12}+\mathbf{r}_{23}+\mathbf{r}_{31})d\mathbf{R}d\boldsymbol{\rho}d\mathbf{r}_{23}d\mathbf{r}_{31}. \tag{44}$$

Substituting $|\Psi|^2$ from Eq. (3) results in

$$w_{L,M}(r_{12})=\frac{1}{(2\pi)^2}\int d\mathbf{q}\int\int d\mathbf{r}_{23}d\mathbf{r}_{31}|P_{L,M}|^2\times\exp\left\{-\frac{1}{18}\sum_{jl}r_{jl}^2+i\mathbf{q}\cdot(\mathbf{r}_{12}+\mathbf{r}_{23}+\mathbf{r}_{31})\right\}. \tag{45}$$

Straightforward calculation shows that

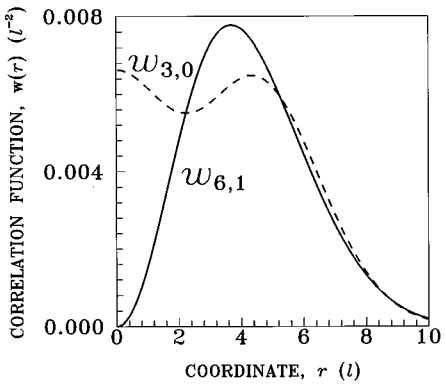

FIG. 7. Radial anyon pair correlation function $w(r)$ for the states $\Psi_{6,1}$ and $\Psi_{3,0}$; $k=0$.

$$w_{6,1}(r)=\frac{r^2}{192\pi}\{1+\tfrac{1}{2}(r/6)^4\}\exp(-r^2/12), \tag{46}$$

$$w_{3,0}(r)=\frac{1}{48\pi}\{1+\tfrac{1}{6}(r/2)^4\}\exp(-r^2/12). \tag{47}$$

Both functions are shown in Fig. 7. The function $w_{6,1}(r)$ has a hard-core behavior, whereas $w_{3,0}(r)$ does not vanish at $r=0$. On the contrary, it reaches its absolute maximum at this point. The second maximum is by the factor 0.97 lower than the main one. Therefore, function $\Psi_{3,0}$ violates the hard-core constraint. Of course, all bottom-state L-odd polynomials with $L\geqslant 9$ show a hard-core behavior.

The above conclusion on the triangular shape of the most probable configuration of the $\Psi_{3,0}$ exciton implies existence of the 120° correlations in the density correlation function.

To investigate these correlations it is convenient to work in the $\boldsymbol{\xi}_j$ variables. The two-particle correlation function $w_{3,0}(\varphi)$ depending on the angle φ between vectors $\boldsymbol{\xi}_1$ and $\boldsymbol{\xi}_2$ can be written as

$$\begin{aligned} w_{3,0}(\varphi) &\propto \int d\boldsymbol{\xi}_1 d\boldsymbol{\xi}_2 d\boldsymbol{\xi}_3 |\widetilde{\Psi}_{3,0}(\boldsymbol{\xi}_1,\boldsymbol{\xi}_2,\boldsymbol{\xi}_3)|^2 \\ &\quad\times\delta(\boldsymbol{\xi}_1+\boldsymbol{\xi}_2+\boldsymbol{\xi}_3)\,\delta(\widehat{\boldsymbol{\xi}_1\boldsymbol{\xi}_2}-\varphi) \\ &\propto \int_0^{2\pi} d\xi_1 d\xi_2 (\xi_1\xi_2)^3(\xi_1^2+\xi_2^2+2\xi_1\xi_2\cos\varphi)^2 \\ &\quad\times\exp\{-(\xi_1^2+\xi_2^2+\xi_1\xi_2\cos\varphi)/3\}. \end{aligned} \tag{48}$$

The δ function takes into account the constraint of Eq. (7), and $\widehat{\boldsymbol{\xi}_1\boldsymbol{\xi}_2}$ stands for the angle between $\boldsymbol{\xi}_1$ and $\boldsymbol{\xi}_2$ expressed in terms of the coordinates of these vectors. Integration over the variables $\boldsymbol{\xi}_j$ in Eq. (48) results in the averaged correlation function; the main contribution comes from the area $\xi_1^2\approx\xi_2^2\approx\xi_3^2\approx 6$ where $|\widetilde{\Psi}_{3,0}|^2$ reaches the maximum. The last integral can be performed in polar coordinates, $\xi_1=\xi\cos(\theta/2)$, $\xi_2=\xi\sin(\theta/2)$, $0\leqslant\theta\leqslant\pi$, and the normalized function $w_{3,0}(\varphi)$ takes the form

$$w_{3,0}(\varphi)=\frac{81}{8\pi}\int_0^{\pi} d\theta\,\frac{\sin^3\theta(1+\sin\theta\cos\varphi)}{(2+\sin\theta\cos\varphi)^5}. \tag{49}$$

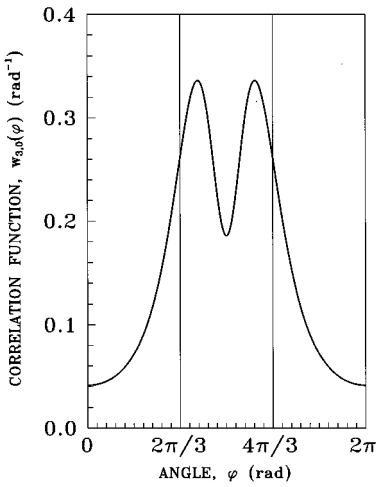

FIG. 8. Normalized anyon pair correlation function $w_{3,0}(\varphi)$ found in the anyon exciton model; $k=0$.

The integration over θ can be performed analytically; however, the final expression is rather cumbersome. The result is plotted in Fig. 8. Two distinct maxima in the vicinity of $2\pi/3$ and $4\pi/3$ reveal 120° correlations in the $\Psi_{3,0}$ state. The maxima are shifted from the angle $2\pi/3$ since the function $\Psi_{3,0}$ vanishes for the collinear configuration of anyons, $\boldsymbol{\xi}_1=-\boldsymbol{\xi}_2$, $\boldsymbol{\xi}_3=0$.

Apalkov and Rashba[41] have found the density-density correlation function, $w^{\mathrm{dd}}_{3,0}(\varphi)$, for the $\nu=2/3$ IQL with a single extra electron. Calculations were performed in the spherical geometry for the $(L_{QP})_{\max}-L_{QP}=3$, $(L_{QP})_z=L_{QP}$ quantum state. The quantity $(L_{QP})_{\max}-L_{QP}$, which is the difference between the three-quasiparticle angular momentum in the spherical geometry, L_{QP}, and the maximum value of this momentum, should be compared to the exciton angular momentum L.[16,17] It is convenient to introduce mean values

$$\rho_1(\vartheta)=\int |\Psi(\boldsymbol{\omega},\boldsymbol{\omega}_2,\ldots\boldsymbol{\omega}_N)|^2 d\boldsymbol{\omega}_2\ldots d\boldsymbol{\omega}_N \tag{50}$$

and

$$\rho_2(\boldsymbol{\omega},\boldsymbol{\omega}')=\int |\Psi(\boldsymbol{\omega},\boldsymbol{\omega}',\boldsymbol{\omega}_3,\ldots\boldsymbol{\omega}_N)|^2 d\boldsymbol{\omega}_3\ldots d\boldsymbol{\omega}_N. \tag{51}$$

Here $\boldsymbol{\omega}_j(\vartheta,\varphi)$ are unit vectors designating the positions of the electrons on the sphere. Electron density depends only on the polar angle ϑ and equals $n_1(\vartheta)=N\rho_1(\vartheta)$, where N is the number of electrons. If one introduces the deviation, $\Delta n(\boldsymbol{\omega})=n(\boldsymbol{\omega})-n_1(\vartheta)$, of the density from its mean value, the density-density correlation function can be written as

$$\begin{aligned} w^{\mathrm{dd}}_{3,0}(\vartheta,\varphi-\varphi') &= \langle\Delta n(\vartheta,\varphi)\Delta n(\vartheta,\varphi')\rangle \\ &= \tfrac{1}{2}N(N-1)\rho_2(\vartheta,\varphi-\varphi')-n_1^2(\vartheta). \end{aligned} \tag{52}$$

In Eq. (52) the polar angles of the vectors $\boldsymbol{\omega}$ and $\boldsymbol{\omega}'$ are chosen equal, $\vartheta=\vartheta'$. Therefore, the correlation function, $w^{\mathrm{dd}}_{3,0}(\vartheta,\varphi)$, is the function of the azimuth φ and depends on

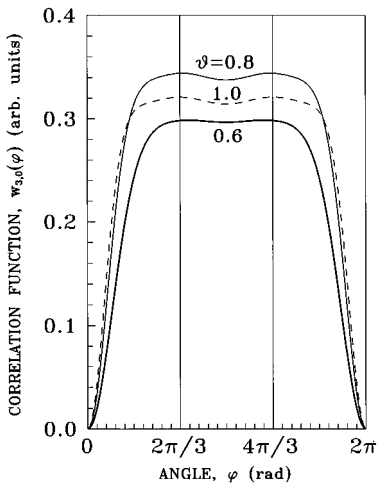

FIG. 9. Electron density correlation function $w^{\rm dd}_{3,0}(\vartheta,\varphi)$ for the $\nu=2/3$ IQL with a single extra electron ($N=15$, the flux $2S=21$). The correlation function is plotted as a function of azimuth φ for three values of the polar angle ϑ = 0.6, 0.8, and 1.0. $\vartheta=0.8$ is close to the maximum of the electron density. Correlations between quasielectrons manifest themselves in the maxima near $\varphi=2\pi/3$ and $4\pi/3$. [Apalkov and Rashba (Ref. 41).]

ϑ as a parameter. In Eq. (52) the singular term proportional to $\delta(\boldsymbol{\omega}-\boldsymbol{\omega}')$ is omitted, as usual, since it makes no contribution to $w^{\rm dd}_{3,0}$ for $\boldsymbol{\omega}\neq\boldsymbol{\omega}'$. The results of calculations are presented in Fig. 9 for three values of ϑ. The value of $\vartheta=0.8$ is close to the maximum of $n_1(\vartheta)$.

Since the anyon exciton wave function $\Psi_{3,0}$ does not depend on h, the data of Figs. 8 and 9 can be compared. There is a striking similarity between them. All three curves in Fig. 9 show flat but distinct maxima near the same values of the argument, $\varphi=2\pi/3$ and $4\pi/3$. These maxima are much flatter than the maxima in Fig. 8. This difference can be attributed to the smearing originating from the quasielectron form factors. Nevertheless, there is no doubt that it is the three quasielectron substructure of the many-electron state $L=3$ which manifests itself in 120° correlations.

Therefore, the state $\Psi_{3,0}$ shows properties intermediate between an anyon exciton and tight exciton. Unfortunately, reliable calculation of $w^{\rm dd}(\vartheta,\varphi-\varphi')$ cannot be performed for the $(L_{QE})_{\max}-L_{QE}=6$ states since their size exceeds the accessible sphere size.

VII. COMPARISON WITH FINITE-SIZE CALCULATIONS

In this section we make a comparison of the AEM with computational results for excitons in the spherical geometry. Three-anyon excitons are expected to appear in two charge conjugate IQL's, $\nu=1/3$ and $\nu=2/3$. Their properties in the semiclassical region, $h\gg1$ and $L\gg1$, should be identical. For intermediate h and L values, excitons of these two liquids are expected to show rather different properties. The data obtained by finite-size computations[16,17] substantiate these expectations.

There are different reasons why $\nu=1/3$ and $\nu=2/3$ excitons are expected to have different properties in the intermediate region. A simple electrostatic reason is a different nonlinear screening of the unit positive charge by these two IQL's. The effect of the screening on the exciton energy spectrum was discussed in Ref. 42. However, there are also different mechanisms resulting in the difference in the properties of these excitons. They are related to rather different form factors and different statistical properties of the quasielectrons of the $\nu=1/3$ and $\nu=2/3$ IQL's. Neglecting spin effects, we can consider electrons as spinless fermions. Then, because of the charge symmetry, the properties of the quasielectrons of the $\nu=2/3$ IQL are identical to the properties of the quasiholes of the $\nu=1/3$ IQL. Therefore, we will start with a comparative study of quasielectrons and quasiholes of the $\nu=1/3$ IQL.

The form factors of charged particles of the $\nu=1/3$ IQL were investigated in a number of papers. The data are summarized in Refs. 34–36. It is known that a quasihole has a narrow profile with a radius up to two magnetic lengths. The density decreases away from the center of a quasihole nearly monotonically. In contrast, a quasielectron has a pronounced density dip at the center, the density maximum at about two magnetic lengths, and the radius of about four magnetic lengths. Therefore, the model of point anyons developed above matches much better the excitons of the $\nu=2/3$ IQL than the excitons of the $\nu=1/3$ IQL.

Another aspect of the problem is related to statistical properties of anyons. In the AEM the effect of the fractional permutational statistics of anyons was taken into account by including the factor $\Pi_{jl}(\overline{z_{jl}})^{\alpha}$ into the Halperin pseudo-wavefunction $\Psi_{L,\mathbf{k}}$, Eq. (3). It was shown in Sec. IV that the effect of this factor can be neglected for $h\gtrsim2$, i.e., in the region where the AEM is expected to be valid. However, one should also take into account the nontrivial populational statistics of anyons. This can be done using the theory of composite fermions[43] and the approach to the dimensionality of the quasiparticle space based on exclusion statistics.[44,45] Bosonic Haldane dimension, d^B_{QP}, is an effective number of the single-quasiparticle states defined in such a way that the usual Bose distribution

$$W_B(d^B_{QP},N_{QP})=(d^B_{QP}+N_{QP}-1)!/(d^B_{QP}-1)!N_{QP}!$$

results in the correct number of states in the Hilbert space of N_{QP} quasiparticles, $W(N_{QP})=W_B(d^B_{QP},N_{QP})$. The number of quasiparticle states, $W(N_{QP})$, can be found by counting the number of states in the Hilbert space of composite fermions.[28,43] If quasiparticles obey Bose statistics, d^B_{QP} does not depend on N_{QP}. By counting the composite fermion number of states in the spherical geometry, it was shown in Ref. 17 that for $\nu=1/m$, m is an integer, the bosonic dimension of quasiholes equals

$$d^B_{QH}=N+1, \tag{53}$$

and the bosonic dimension of quasielectrons equals

$$d^B_{QE}=(N+1)-2(N_{QE}-1). \tag{54}$$

Here N is the number of electrons. These equations are consistent with the diagonal coefficients of the exclusion statistics of quasiholes and quasielectrons ($1/m$ and $2-1/m$, respectively), found by different authors.[46–48]

Equations (53) and (54) indicate that quasiholes show a bosonic behavior, while quasielectrons are a subject of the constraint which is even more restrictive than the constraint imposed by Fermi statistics. These conclusions were supported[17] by counting the maximum value of the angular momentum, $(L_{QP})_{\max}$, for the system of N_{QP} quasiparticles. It is equal to

$$(L_{QH})_{\max}=N_{QH}N/2 \tag{55}$$

for N_{QH} quasiholes, and to

$$(L_{QE})_{\max}=N_{QE}N/2-N_{QE}(N_{QE}-1) \tag{56}$$

for N_{QE} quasielectrons. Since $N/2$ is the angular momentum of a single quasiparticle,[21] Eq. (55) confirms the bosonic behavior of quasiholes, whereas Eq. (56) confirms the existence of the restriction on the population of single-quasiparticle states by quasielectrons. He *et al.*[27] were the first to discover this restriction by means of numerical calculations and to propose Eqs. (53) and (54). They attributed the restriction to the hard-core constraint for quasielectrons having a dynamical (short-range repulsion) rather than statistical origin.

For a macroscopic system, $N\gg 1$, Eqs. (53) and (54) give coinciding results, $d^B_{QE}\approx d^B_{QH}\approx N$, in the dilute limit, $N_{QP}\ll N$. However, in an exciton the quasiparticles are confined inside the volume about πr^2, where r is the exciton radius. Therefore, the second term of Eq. (54) which signifies the deviation from the bosonic behavior of quasielectrons, can be of importance.

Quasielectrons of the $\nu=2/3$ IQL are described by Eqs. (53) and (55). Therefore, the population of single-quasiparticle states obeys the Bose statistics, and Eq. (3) for wave functions is absolutely adequate since it includes polynomials $P_{L,M}$ symmetrical in variables $\overline{z_j}$. For this reason, and also taking into account narrow form factors of quasielectrons of the $\nu=2/3$ IQL, one can conclude that the $\nu=2/3$ IQL is the best candidate for comparison with the AEM. We believe that the criterion $h\gtrsim 2$, established in Sec. V by evaluating the density $D_\lambda(r,0)$, is applicable to the $\nu=2/3$ IQL.

The situation is more involved for the $\nu=1/3$ IQL. Quasielectrons in this case are described by Eqs. (54) and (56). One can apply Eq. (54) to the area inside an exciton and order that $d^B_{QE}\geqslant N_{QE}=3$, which results in $N\geqslant 6$. The number of electrons inside an exciton can be evaluated as $N\approx \pi r^2/2\pi$. Evaluating the exciton radius r as $r\approx r_{12}/\sqrt{3}$ and using the classical equation (35), one comes to the criterion $h\gtrsim 5$. A wide quasielectron form factor imposes a similar restriction on h. Since the reliable finite-size computations can be performed only for $h\lesssim 2$, the prospects for a quantitative comparison of the results obtained by both approaches seem less favorable for the $\nu=1/3$ IQL than for the $\nu=2/3$ IQL. However, we feel that the above rigid criterion relaxes considerably when a qualitative description of the spectrum-bottom states is concerned.

We are now in position to compare the basic results of the AEM with the computational results for finite-size systems. The basic statement of the theory of anyon excitons, that the charge fractionalization results in a multiple-branch energy spectra of excitons,[11,22] was confirmed by finite-size computations performed for both $\nu=1/3$ and $\nu=2/3$ IQL's. Actually, it provides the basic idea for representing the energy spectra obtained in the spherical geometry for a discrete set of L values in the form of exciton branches $\varepsilon_\lambda(\mathbf{k})$.

We begin with summarizing some results obtained in Ref. 17 by finite-size calculations for excitons of the $\nu=2/3$ IQL and compare them with the results obtained in this paper in the framework of the AEM. Classification of excitons in terms of tight and anyon excitons is used, cf. Sec. I.

1. *Number of exciton species*. Anyon exciton is a bound state of a three-quasielectron complex from the low-energy (anyon) sector[27,28] and a hole. The angular momentum of the exciton, L, is equal to $L^*=(L_{QE})_{\max}-L_{QE}$, where L_{QE} is the angular momentum of the complex, and $(L_{QE})_{\max}$ is the maximum value of this momentum which can be found from Eq. (55). Therefore, the number of exciton species is equal to the number of the three-quasielectron complexes in the low-energy sector, and L^* should be compared to the exciton angular momentum L of the AEM. Only a single three-quasielectron complex exists if the angular momentum L^* equals $L^*=0$, 2, 3, 4, 5, or 7. The complex $L^*=1$ is absent because composite fermions obey Fermi statistics. For $L^*\geqslant 6$ the number of L-even states increases by one (see Fig. 1 in Ref. 17).

These properties are in a complete agreement with the classification of the polynomials $P_{L,M}$ of Sec. II, Eqs. (9) and (10). The $L=1$ exciton is absent because of the constraint of Eq. (2).

2. $L=0$ *branch*. Despite the fact that the $L=0$ exciton appears, according to its quantum number, as the first state in the series of anyon excitons, it possesses rather special properties. This exciton originates from the $L^*=0$ three-quasielectron complex, which is quite dense, and the energy of this complex is high. It is nearly the same as the energy of some states from the next sector. These data imply that the $L=0$ anyon exciton actually merges with the $L=0$ tight exciton. Because of these arguments, the $L=0$ exciton was assigned in Ref. 17 as a tight exciton rather than an anyon one. This assignment is supported by an independent argument. $L=0$ excitons of the $\nu=2/3$ and $\nu=1/3$ IQL's show nearly identical properties, whereas the anyon exciton assignment of the latter entity is excluded by the symmetry arguments based on the composite fermion theory.[16]

The shape of the $L=0$ exciton density distribution of Fig. 3 is in agreement with this assignment. The magnitude of $D_0(0,0)$ exceeds the maximum density compatible with the AEM; see the discussion at the beginning of Sec. V.

3. *Electron density*. For a system with a single extra electron against a background of the $\nu=2/3$ IQL, the electron density has a pronounced maximum at $r=0$ if $L^*=0$, 2, or 4. The $L^*=3$ state is the first state with a craterlike electron density distribution having a density dip at $r=0$ (see Fig. 2 in Ref. 17). The crater shape of the density indicates the charge fractionalization.

These data are in a qualitative agreement with the electron density distributions of Fig. 3 for excitons having angular momenta $L=0$, 2, 3, and 4. The general shape of the curves is the same, but there are differences in the magnitudes of the densities at $r=0$. Since wave functions of these excitons do

not depend on h, electron densities for the exciton and three-quasielectron states with the angular momenta $L=L^*$, respectively, can be compared.

4. *Bottom states*. $L=0$ exciton remains the bottom state in the whole area $h\lesssim 2$. $L=2$, $L=3$, and $L=6$ excitons move down to the spectrum bottom, but they start competing with the $L=0$ exciton only for $h\approx 2.5$ when the accuracy of finite-size calculations becomes ambiguous. The $L=4$ exciton is also seen in the low-energy part of the spectrum but never reaches the spectrum bottom.[17,41]

These data are in agreement with Fig. 4 where the sequence of the first bottom states includes $L=0$, 2, 3, and 6.

5. *Charge fractionalization: density correlation function*. It was shown in Sec. VI that $w_{3,0}(\varphi)$ reveals 120° correlations both for the many-electron and AEM wave functions. These correlations signal the charge fractionalization.

6. *Intrinsic angular momenta of anyons*. There is a convincing one-to-one correspondence between the excitons of many-electron systems having angular momenta $L\leqslant 6$ in the spherical geometry and the excitons of the AEM with the same values of the z projections of the angular momentum. Therefore, our data provide no indication of the existence of the intrinsic angular momenta of anyons.[49] On the contrary, our data are in agreement with the recent conjecture on the absence of anyon spins in the plane limit.[50]

The AEM predicts identical exciton spectra for the $\nu=2/3$ and $\nu=1/3$ IQL's. However, finite-size calculations[16,17] result in a rather different symmetry of the low-energy exciton states for $h\lesssim 2$. The exact classification of the exciton states based on the composite fermion theory shows that only $L=3$ and $L\geqslant 5$ anyon excitons can exist in the $\nu=1/3$ IQL.[16] This conclusion is supported by numerical data. Therefore, a challenging question arises: Why are $L=2$ and $L=4$ excitons of the AEM missing from the many-electron spectra of the $\nu=1/3$ IQL? We argue that these excitons are excluded because of their small bosonic dimension which cannot accommodate three quasielectrons.

In what follows we compare the results of the finite-size computations of Ref. 16 for the $\nu=1/3$ IQL with the AEM data.

1. *Excluded states*. Finite-size calculations and composite fermion theory show that anyon excitons of the $\nu=1/3$ IQL can only possess angular momenta $L=3$ and $L\geqslant 5$. All excitons with $L=0$, 1, 2, and 4 can only appear as tight excitons. The $L=0$ tight exciton forms the spectrum bottom for $h\lesssim 2$, but there are no low-energy $L=2$ and $L=4$ excitons.

It seems probable that there can exist only one, $L=0$, tight exciton near the spectrum bottom. Therefore, it is necessary to understand why $L=2$ and $L=4$ excitons of the AEM, which possess low-energies, do not appear as anyon-excitons in many-electron systems. The criterion $d^B_{QE}\geqslant N_{QE}$ results in the minimum anyon-exciton radius of $r_{\min}\approx 2\sqrt{3}$. It is seen in Fig. 3 that the criterion $r\gtrsim r_{\min}$ is violated for $L=2$ and $L=4$ excitons. Therefore, we attribute the exclusion of the $L=2$ and $L=4$ exciton states from the many-electron spectrum to the reduction of the bosonic dimension of the quasielectron space because of the second term of Eq. (54).

2. *Bottom states.* The tight $L=0$ exciton remains the bottom state up to $h\approx 2$ when the $L=3$ anyon exciton reaches the bottom. $L=5$ and $L=6$ excitons start to compete with the $L=0$ exciton only for $h\approx 3$ when the accuracy of finite-size calculations is low.

The data are in agreement with Fig. 4.

3. *Electron density distribution for* $\mathbf{k}=0$ *excitons*. Tight excitons have narrow electron density distributions. The density of the $L=0$ exciton is sharply peaked at $r=0$. $L=3$ and $L=5$ anyon excitons show pronounced density dips at $r=0$ and two maxima of the density. It was hypothesized[16] that the $r=0$ dip originates from the dip in the quasielectron form factor, whereas the two-maxima shape indicates the existence of a two-anyon core and one split-off anyon. It is remarkable that the density distribution in the $L=3$ and $L=5$ excitons only weakly depends on h.

Weak h dependence of the density distribution for $L=3$ and $L=5$ excitons is in agreement with the existence of a single polynomial $P_{L,M}$ for $L\leqslant 6$, Sec. II. Splitting of the exciton shell of a $\mathbf{k}=0$ exciton cannot be described within the framework of the point-anyon AEM.

4. *Dependence of the density distribution on* $\mathbf{k}$. When k increases, the $r=0$ dip in the electron density of the $L=3$ exciton transforms into a narrow maximum, and the density distribution acquires a three-maxima shape. It was proposed[16] that in this region of k values an exciton consists of a single-anyon core and a two-anyon shell.

Splitting off of anyons from the core with increasing k is in a qualitative agreement with Fig. 6.

VIII. CONCLUSION

The model of anyon exciton developed and solved in the paper includes three quasielectrons (anyons) and one hole. It is applicable to exciton spectra of two charge conjugate IQL's, $\nu=1/3$ and $\nu=2/3$, and is exact in the limit of a large separation between electron and hole confinement planes, $h\gg l$.

Anyon excitons possess multiple-branch energy spectra, $\varepsilon_\lambda(\mathbf{k})$. An exciton is described by a 2D momentum $\mathbf{k}$ and two internal quantum numbers λ which numerate exciton branches. One of these quantum numbers can be chosen as the exciton angular momentum, L, in the $\mathbf{k}=0$ state.

A full set of basis functions was chosen with a proper account of the magnetic translational symmetry and permutational symmetry. The functions include two types of polynomials symmetric in anyon permutations; one of them, apparently, was considered for the first time. Analytic expressions for all matrix elements were derived. As a result, exact expressions for the energy spectrum of a four-particle system were found for $\mathbf{k}=0$. All exciton states with even angular momenta $L<6$ and odd momenta $L<9$ are nondegenerate, and their wave functions are completely determined by symmetry requirements. This property manifests itself in finite-size data in a weak h dependence of the electron density distribution. Properties of $\mathbf{k}\neq 0$ excitons were investigated by numerical solution of the Schrödinger equation.

The AEM is not applicable for small h values, $h\lesssim 2l$. However, the analysis of the internal criteria of the AEM and comparison with the finite-size data show that it gives satis-

factory results for $h \approx 2l$, especially for excitons of the $\nu = 2/3$ IQL. Finite-size computations which are reliable for $h \lesssim 2l$, and the AEM, whose accuracy increases with h, constitute two supplementary approaches which match at $h \approx 2l$. According to the AEM, exciton states with the angular momenta obeying the superselection rule $L = 3m$, where $m \geqslant 2$ is an integer, form the sequence of the bottom states for $h \gtrsim 2l$. All these states are hard-core states, i.e., their wave functions turn into zero if any two of the anyon coordinates coincide. The equilateral anyon configurations are the most probable ones. Angular momenta L of the bottom states increase as h^2, and the size of these states as h. The tight $L = 0$ state is the bottom state for $h \lesssim 2l$, whereas the $L = 3$ state, which possesses the properties of both anyon and tight excitons, can reach the bottom for $h \approx 2l$.

Anyon substructure of excitons manifests itself in their different properties. First, the multiple-branch energy spectrum originates because of the existence of the internal degrees of freedom. Second, for $\mathbf{k} = 0$ excitons a craterlike shape of the electron density distribution with a pronounced dip near the hole signals the existence of the charge fractionalization. Third, 120° correlations in the electron density were found both in the framework of the AEM and in finite-size data. Fourth, for $\mathbf{k} \neq 0$ excitons a spectacular splitting of the electron density into bunches provides a direct manifestation of the fractional charge substructure.

AEM results in identical low-energy spectra for the excitons of the $\nu = 1/3$ and $\nu = 2/3$ IQL's. This result is definitely correct in the $h \gg l$ limit. However, finite-size data suggest that in the intermediate region, $h \approx l$, the $\nu = 1/3$ IQL possesses less anyon-exciton branches than the $\nu = 2/3$ IQL. Following Ref. 17, we attribute this phenomenon to the difference in the populational statistics of the quasielectrons of the charge conjugate IQL's. Anyon statistics enters into the theory in two ways. First, through the fractional-power factors in the wave function; they ensure correct interchanging statistics. Second, through the populational statistics. We have shown that the first mechanism can be neglected for $h \gtrsim 2l$, whereas the second one is of a critical importance in the intermediate region. It follows from the composite fermion theory that quasielectrons of the $\nu = 2/3$ IQL obey bosonic populational statistics. As a result, quantum numbers of anyon excitons found from the AEM and from the finite-size data exactly coincide. In contrast, the bosonic dimension, d^B_{QE}, of the quasielectron space of the $\nu = 1/3$ IQL rapidly decreases with the number of quasielectrons, N_{QE}. The condition $d^B_{QE} \geqslant N_{QE}$, written for the area about the exciton size, eliminates the exciton states of the AEM with the angular momenta $L = 2$ and $L = 4$ from the many-electron spectrum and brings in agreement the AEM and many-electron data. Therefore, for $h \approx 2l$ the AEM supplemented with anyon statistics arguments matches the many-electron data for both IQL's and sheds light on the origin of the difference in their exciton spectra. The above arguments are rather general and can be applied to different problems of the theory of the bound states of several anyons.

Comparison of the AEM and finite-size data for $\nu = 2/3$ IQL provides no indication of the existence of the intrinsic angular momenta (spins) of anyons.

In conclusion, the anyon exciton model unveils the general pattern of the exciton spectra of IQL's. It predicts the properties of excitons in the large h limit, $h \gg l$, and is in agreement with finite-size data in the intermediate region, $h \approx 2l$. The theory suggests that the region $h \gtrsim 2l$ is most favorable for investigating the anyon substructure of excitons in optical experiments.

ACKNOWLEDGMENTS

We are grateful to A. L. Efros and Y.-S. Wu for discussions and comments, and to E. V. Tsiper for suggestions related to L-odd polynomials. E.I.R. acknowledges the support of the San Diego Supercomputer Center where finite-size computations were performed. We also acknowledge the support of the QUEST of the UCSB by subagreement KK3017.

[1] R. B. Laughlin, Phys. Rev. Lett. **50**, 13 (1983).
[2] D. C. Tsui, H. Stormer, and A. C. Gossard, Phys. Rev. Lett. **48**, 1559 (1982).
[3] B. I. Halperin, Phys. Rev. Lett. **52**, 1583 (1984).
[4] D. Arovas, J. R. Schrieffer, and F. Wilczek, Phys. Rev. Lett. **53**, 722 (1984).
[5] I. Kukushkin, V. Timofeev, K. von Klitzing, and K. Ploog, Festkörperprobleme **28**, 21 (1988); D. Heiman, B. B. Goldberg, A. Pinczuk, C. W. Tu, A. C. Gossard, and J. H. English, Phys. Rev. Lett. **61**, 605 (1988); A. J. Turberfield, S. H. Heines, P. A. Wright, R. A. Ford, R. G. Clark, J. F. Ryan, J. J. Harris, and C. T. Foxon, Phys. Rev. Lett. **65**, 637 (1990); E. M. Goldis, S. A. Brown, R. B. Dunford, A. G. Davies, R. Newbury, R. G. Clark, P. E. Simmonds, J. J. Harris, and C. T. Foxon, Phys. Rev. B **46**, 7957 (1992).
[6] A. Pinczuk, B. S. Dennis, L. N. Pfeiffer, and K. West, Phys. Rev. Lett. **70**, 3983 (1993).
[7] S. M. Girvin, A. H. MacDonald, and P. M. Platzman, Phys. Rev. **33**, 2481 (1986).
[8] A. H. MacDonald, E. H. Rezayi, and D. Keller, Phys. Rev. Lett. **68**, 1939 (1992).
[9] B.-S. Wang, J. L. Birman, and Z.-B. Su, Phys. Rev. Lett. **68**, 1605 (1992).
[10] V. M. Apalkov and E. I. Rashba, Pis'ma Zh. Eksp. Teor. Fiz. **55**, 38 (1992) [JETP Lett. **55**, 37 (1992)].
[11] E. I. Rashba and M. E. Portnoi, Phys. Rev. Lett. **70**, 3315 (1993).
[12] X. M. Chen and J. J. Quinn, Phys. Rev. B **50**, 2354 (1994).
[13] I. V. Kukushkin, R. J. Haug, K. von Klitzing, K. Eberl, and K. Tötemeyer, Phys. Rev. B **50**, 11 259 (1994).
[14] E. I. Rashba and V. M. Apalkov, in *Optical Phenomena in Semiconductor Structures of Reduced Dimensions*, edited by D. J. Lookwood and A. Pinczuk, Vol. 248 of *NATO Advanced Study Institute, Series B: Physics* (Kluwer, Dordrecht, 1993), p. 63.
[15] D. Heiman, F. Plentz, A. Pinczuk, L. N. Pfeiffer, and K. W. West, Bull. Am. Phys. Soc. **41** (1), 76 (1996).
[16] V. M. Apalkov, F. G. Pikus, and E. I. Rashba, Phys. Rev. B **52**, 6111 (1995).

[17] V. M. Apalkov and E. I. Rashba, Solid State Commun. **95**, 421 (1995).
[18] X. M. Chen and J. J. Quinn, Phys. Rev. Lett. **70**, 2130 (1993).
[19] E. H. Rezayi, in *Optical Phenomena in Semiconductor Structures of Reduced Dimensions* (Ref. 14), p. 79.
[20] V. M. Apalkov and E. I. Rashba, Phys. Rev. B **46**, 1628 (1992).
[21] F. D. M. Haldane, Phys. Rev. Lett. **51**, 605 (1983).
[22] M. E. Portnoi and E. I. Rashba, Mod. Phys. Lett. B **9**, 123 (1995).
[23] L. P. Gor'kov and I. E. Dzyaloshinskii, Zh. Eksp. Teor. Fiz. **53**, 717 (1967) [Sov. Phys. JETP **26**, 449 (1968)].
[24] E. I. Rashba and V. M. Apalkov, *Conference Book of the 11th International Conference on High Magnetic Fields in Semiconductor Physics* (MIT, Cambridge, 1994), p. 648.
[25] J. Zang and J. L. Birman, Phys. Rev. B **51**, 5574 (1995).
[26] X. M. Chen and J. J. Quinn, Phys. Rev. B **51**, 5578 (1995).
[27] S. He, X.-C. Xie, and F.-C. Zhang, Phys. Rev. Lett. **68**, 3460 (1992).
[28] G. Dav and J. K. Jain, Phys. Rev. Lett. **69**, 2843 (1992).
[29] N. R. Cooper and D. B. Chklovskii, Phys. Rev. B (to be published).
[30] R. K. Kamilla, X. G. Wu, and J. K. Jain, Solid State Commun. **99**, 289 (1996).
[31] Y.-S. Wu, Phys. Rev. Lett. **52**, 2103 (1984); **53**, 111 (1984).
[32] G. Birkhoff and S. Mac Lane, *A Survey of Modern Algebra* (Macmillan, New York, 1977).
[33] D. Endesfelder and O. Terzidis, Z. Phys. B **87**, 51 (1992).
[34] T. Chakraborty and P. Pietiläinen, *The Quantum Hall Effect* (Springer-Verlag, Berlin, 1995).
[35] P. Béran and R. Morf, Phys. Rev. B **43**, 12 654 (1991), and references therein.
[36] U. Girlich and M. Hellmund, Phys. Rev. B **49**, 17 488 (1994), and references therein.
[37] I. S. Gradshteyn and I. M. Ryzhik, *Table of Integrals, Series and Products* (Academic, New York, 1980).
[38] A. H. MacDonald and E. H. Rezayi, Phys. Rev. **42**, 3224 (1990); V. M. Apalkov and E. I. Rashba, Pis'ma Zh. Eksp. Teor. Fiz. **54**, 155 (1991) [JETP Lett. **54**, 155 (1991)].
[39] N. Sivan and S. Levit, Phys. Rev. B **46**, 3953 (1992).
[40] F. C. Zhang, V. Z. Vulovic, Y. Guo, and S. Das Sarma, Phys. Rev. B **32**, 6920 (1985); E. H. Rezayi and F. D. M. Haldane, *ibid.*, p. 6924.
[41] V. M. Apalkov and E. I. Rashba (unpublished).
[42] T. V. Tatarinova, E. I. Rashba, and A. L. Efros, Phys. Rev. B **50**, 17 349 (1994).
[43] J. K. Jain, Adv. Phys. **41**, 105 (1992).
[44] F. D. M. Haldane, Phys. Rev. Lett. **67**, 937 (1991).
[45] Y.-S. Wu, Phys. Rev. Lett. **73**, 922 (1994).
[46] M. D. Johnson and G. S. Canright, Phys. Rev. B **49**, 2947 (1994).
[47] J. Yang, Phys. Rev. B **50**, 11 196 (1994).
[48] W.-P. Su, Y.-S. Wu, and J. Yang, Phys. Rev. Lett. **77**, 3423 (1996).
[49] D.-H. Lee and X.-G. Wen, Phys. Rev. B **49**, 11 066 (1994).
[50] T. Einarsson, S. L. Sondhi, S. M. Girvin, and D. P. Arovas, Nucl. Phys. B **441**, 515 (1995).